



**INVESTIGATION OF THE ATMOSPHERIC PROPAGATION OF ALKALI
LASERS IN A MARITIME ENVIRONMENT USING TUNABLE DIODE LASER
ATMOSPHERIC SPECTROSCOPY**

THESIS

Matthew R. Guy, 2 Lt, USAF

AFIT-ENP-13-M-12

**DEPARTMENT OF THE AIR FORCE
AIR UNIVERSITY**

AIR FORCE INSTITUTE OF TECHNOLOGY

Wright-Patterson Air Force Base, Ohio

**DISTRIBUTION STATEMENT A.
APPROVED FOR PUBLIC RELEASE; DISTRIBUTION IS UNLIMITED.**

The views expressed in this thesis are those of the author and do not reflect the official policy or position of the United States Air Force, Department of Defense, or the United States Government. This material is declared a work of the United States Government and is not subject to copyright protection in the United States.

AFIT-ENP-13-M-12

INVESTIGATION OF THE ATMOSPHERIC PROPAGATION OF ALKALI LASERS
IN A MARITIME ENVIRONMENT USING TUNABLE DIODE LASER
ATMOSPHERIC SPECTROSCOPY

THESIS

Presented to the Faculty

Department of Engineering Physics

Graduate School of Engineering and Management

Air Force Institute of Technology

Air University

Air Education and Training Command

In Partial Fulfillment of the Requirements for the

Degree of Master of Science in Applied Physics

Matthew R. Guy, B.S.

Second Lieutenant, USAF

March 2013

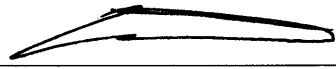
DISTRIBUTION STATEMENT A.
APPROVED FOR PUBLIC RELEASE; DISTRIBUTION IS UNLIMITED.

AFIT-ENP-13-M-12

INVESTIGATION OF THE ATMOSPHERIC PROPAGATION OF ALKALI LASERS
IN A MARITIME ENVIRONMENT USING TUNABLE DIODE LASER
ATMOSPHERIC SPECTROSCOPY


Matthew R. Guy, B.S.
Second Lieutenant, USAF

Approved:




Glen Perram, PhD (Chairman)

7 Mar 13
Date



Kevin Gross, PhD (Member)

7 Mar 13
Date



Steven Fiorino, PhD (Member)

7 MAR 13
Date

Abstract

A field deployable Tunable Diode Laser Atmospheric Spectroscopy (TDLAS) device has been used to investigate the atmospheric absorption of Diode Pumped Alkali Laser (DPAL) wavelengths at a distance of 2,000 meters in a maritime environment. The spectral regions surrounding the cesium (Cs) and rubidium (Rb) DPAL emission lines, 890 to 910 nanometers and 790 to 800 nanometers respectively, were examined in order to determine the effects of absorption by the $(0\ 0\ 0) \rightarrow (0\ 0\ 3)$ and $(0\ 0\ 0) \rightarrow (1\ 0\ 2)$ water vapor vibrational bands.

Spectral data for the Cs spectral region were analyzed to determine temperature estimates of between 6.60 to 30.02° C with statistical errors of between 0.1 and 1.14° C and concentration estimates of between 2.42 to 3.51 x 10¹⁷ cm⁻³ with error bounds 0.011 and 0.001 x 10¹⁷ cm⁻³ over the 9 day span of data collection. Temperature and pressure estimates were within 6% and 25%, respectively, of those reported by the Davis Vantage Pro2 portable weather station used to collect on site meteorological data for the experiment.

The observed spectra were compared to data previously collected at 150 and 1,000 meters and the differences were investigated. The strength of the absorption features at the 150 and 2,000 meters scaled primarily with path length as the water vapor concentration only varied slightly between the two experiments. The strengths at 1,000 and 2,000 meters scaled in part with path length and in part with concentration, with the combination of these effects only differing from the actual intensity ratio by 15%.

AFIT-ENP-13-M-12

The rotational dependence of broadening rates was investigated. By analyzing the widths of the $[1\ 1\ 0] \rightarrow [2\ 1\ 1]$ and $[6\ 2\ 5] \rightarrow [7\ 2\ 6]$ rotational transitions in the $(0\ 0\ 0) \rightarrow (0\ 0\ 3)$ vibrational band of water vapor, it was found that the observed linewidths were approximately 25% higher than those reported in the High resolution TRANsmision molecular absorption (HITRAN) 2008 database and that the scaling ratio of the observed rates was 5% below the ratio of the reported values.

For my mother and father, for all of their love and support.

Acknowledgments

I would like to express my sincere appreciation to my research advisor, Dr. Glen Perram for his advice, guidance, and support over the course of my thesis research. His insight was invaluable in ensuring the successful completion of this effort. I would also like to thank the other members of my committee, Dr. Kevin Gross and Dr. Steven Fiorino, for their input and assistance throughout my endeavor. Finally, I would like to thank my sponsor, the High Energy Laser Joint Technology Office, for the opportunity to undertake this research. I am extremely grateful to all parties who enabled me to successfully complete my thesis, it has been greatly appreciated.

Matthew R. Guy

Table of Contents

	Page
Abstract	iv
Acknowledgments.....	vii
Table of Contents	viii
List of Figures	x
List of Tables	xiii
I. Introduction	1
II. Background	4
TDLAS Background	4
H ₂ O Spectroscopy	4
Molecular Absorption	5
Lineshapes.....	6
Molecular Scattering.....	10
Turbulence	11
III. Equipment	12
IV. Experiment.....	14
Physical Setup.....	14
Experimental Procedure.....	19
Atmospheric Absorption Spectra.....	21
Long Term Single Frequency Baseline Monitoring	22
Long Term Single Line Monitoring.....	23
Meteorological Data.....	23
Testing Schedule.....	24
V. Results.....	26
Meteorological Data.....	26
Atmospheric Absorption Spectra.....	29
Broad Cesium Region Spectra	29
Narrowed Cesium Region.....	31
Fit Correlations with Meteorological Data	32
Comparison with Previous Work.....	36
Rotational Dependence of Broadening Rates	39

VI. Conclusions and Recommendations	42
Conclusions of Research.....	42
Recommendations for Future Research	44
Appendix A.....	47
Appendix B.....	61
Bibliography	67
Vita.....	69

List of Figures

Figure	Page
1	Three vibrational modes of a water molecule, the symmetric stretch (left), the bend (center), and the asymmetric stretch (right)..... 5
2	Diagram of the test site showing the TDLAS main site to the north and the mirror site to the south, separated by 1016 m. Exact coordinates for each site are shown. Machodoc River runs between the sites, beginning to the west and emptying into the Potomac River to the east. 14
3a	Diagram of the TDLAS main site. The Dahlgren Naval Surface Warfare Center is located to the north and the river is to the south..... 16
3b	Picture of the TDLAS main site showing the physical setup of the test equipment at the main test site. The control tent is on the left, the CONEX storage container is in the middle, and the box truck containing the majority of the test equipment is on the right. The BLS 900 Scintillometer receiver and processing unit are located in front of the CONEX..... 17
4a	Diagram of the mirror dock site. The dock extends into the river from the south 18
4b	A picture of the mirror site showing the physical layout of the test equipment. On the left is the BLS 900 Scintillometer transmitter, in the center is the 6” turning mirror, and on the right is a crude retro reflector array borrowed from Dahlgren NSWC. A large foam rectangle with reflective strips was taped to the shed behind the test equipment to aid in alignment. 19
5a	C_n^2 measurements collected over the duration of the experiment. The turbulence values cycle from $\sim 5 \times 10^{-13}$ at night to $\sim 5 \times 10^{-15}$ in the afternoon just prior to sunset..... 26
5b	Turbulence measurements for 21 October, highlighting the drastic rise in turbulence immediately following sunset. 27
6	Particle counts for a seven hour block of time on 22 October 2012. This sample includes a count fall off around 17:15 corresponding to the alcohol cartridge in the particle counter failing as well as a spike of over 50,000 particles/cm ³ corresponding to the spray of insect repellent near the collector inlet. Typical particle counts were on the order of 1,000 to 2,000 particles/cm ³ 28

7	Atmospheric absorption spectrum of the entire 20 nm range of the New Focus Velocity 6318 Tunable Diode Laser. The majority of the spectrum is made up of the rotational structure of the (0 0 0)→(0 0 3) vibrational transition with some small contributions by the (000)→(102) transition.	29
8	0.3 nm sample of the atmospheric absorption spectrum collected over the 6 nm range immediately surrounding the Cs D ₁ doublet. ν_{ref} is the energy of the lowest frequency line of the Cs doublet, 11178.112 cm ⁻¹ . The dashed line represents the LBLRTM fit to the collected data, displayed as black points. The Cs doublet appears as a dotted line and was excluded from the atmospheric model fit as Cs parameters are not included in atmospheric databases. The gaps in the spectrum are a product of the tunable laser failing to completely overlap consecutive scans.	31
9a	Temperature measurements from the Davis Vantage Pro2 weather station (dark grey line), national weather station in Quantico, VA (dashed line), and spectral fit estimates (data markers) for the 9 day duration of data collection.	33
9b	Temperature measurements from the Davis Vantage Pro2 weather station (dark grey line), national weather station in Quantico, VA (dashed line), and spectral fit estimates (data markers) for the 9 day duration of data collection.	33
10	Fit estimates and weather station data for temperature on 17 October 2012. Vertical error bars correspond to 95% statistical errors from the fits and horizontal error bars represent the period of time covered by each piece of the collection. The solid grey line represents the Davis weather station data and the dashed line represents the temperature data from the national weather station at Quantico.	35
11	Atmospheric absorption spectra collected over the Cs D ₁ spectral region at 150 m (black), 1,000 m (dark gray), and 2,000 m (light gray). The D ₁ doublet is included in the spectrum collected at 150 m. The increase in baseline noise is clear as the experimental path length is increased, with a dramatic rise going to 2,000 m due to a lack of signal averaging as well as additional platform jitter.	37

12	Absorption lines corresponding to the [1 1 0] → [2 1 1] (light gray) and [6 2 5] → [7 2 6] (dark gray) rotational transitions within the vibrational (0 0 0) → (0 0 3) band, overlaid and normalized to a peak intensity of 1. An LBLRTM fit for each line is superimposed on the data, with the dotted line corresponding to the J = 2 line and the dashed line corresponding to the J = 7 line. Noise in the top of each data set is due to absorbance beyond the detectable limit of the lock-in amplifiers.	40
13	Atmospheric absorption spectrum in the region surrounding the Cs DPAL emission line, taken from 1545 to 1700 on 17 October 2012. The scan ranges from 11,140 to 11,210 cm ⁻¹ and contains ~30 absorption line, a number of which are obscured by baseline noise.	61
14	Atmospheric absorption spectra from 12,480 to 12,530 cm ⁻¹ collected from 1628 to 1909 on 19 October 2012. This spectrum contains ~25 weak H ₂ O absorption lines, many of which are obscured by the noise in the baseline.	62
15	Atmospheric absorption spectra from 12,554 to 12,570 cm ⁻¹ collected from 2159 on 19 October 2012 to 0050 on 20 October 2012. The lower noise level is due to the signal averaging used. With 6 scans per piezo range, the signal to noise ratio was improved significantly.	63
16	Atmospheric absorption spectra in the Cs DPAL emission region, from 11,150 to 11,210 cm ⁻¹ , collected from 1905 to 2136 on 22 October 2012. This spectrum contains ~30 strong H ₂ O absorption lines, some of which are obscured by the noise in the baseline, as well as the Cs doublet located at ~11,182 cm ⁻¹	64
17	Sample of data collected in the Rb region, from 12,555 to 12,600 cm ⁻¹ , on 23 October 2012 from 1515 to 1542 consisting of ~25 weak H ₂ O absorption lines as well as the Rb D ₁ emission lines at ~12,578cm ⁻¹	65
18	Atmospheric absorption spectra from 12,525 to 12,550 cm ⁻¹ collected from 1551 to 1705 on 23 October 2012. This spectrum contains over 30 weak H ₂ O absorption lines, many of which are obscured by the noise in the baseline.	66

List of Tables

Table		Page
1	Schedule showing what data was collected on each day of the test. Data was collected between 16 October and 25 October, with a day before and after this for set up and packing respectively. Cs and Rb Full represent days where full spectra were collected for each species. Cs Long represents a long term absorption line measurement and Rb Long represents a long term baseline monitoring collection.....	25
2	Scan times, fit estimates, 95% confidence bounds (\pm), Davis weather station, and percent error for each scan analyzed.....	36
3	Observed concentration and absorption values for 150, 1,000, and 2,000 meter collections. All ratios are with respect to the relevant values at 2,000 meters. The ratio product is determined by multiplying the path ratio by the concentration ratio.....	39
4	HITRAN 08 data for the lines observed in the 890 to 910 nm range surrounding the Cs D1 emission line.....	47

INVESTIGATION OF THE ATMOSPHERIC PROPAGATION OF ALKALI LASERS
IN A MARITIME ENVIRONMENT USING TUNABLE DIODE LASER
ATMOSPHERIC SPECTROSCOPY

I. Introduction

Significant effort into the development of Diode Pumped Alkali Lasers (DPAL's) began in 2003 with Krupke's demonstration of the first 3 level rubidium (Rb) laser [1]. After this first demonstration, which used a titanium sapphire laser as the pump source, work began on semiconductor laser pumped systems, resulting in the first demonstration of a true DPAL by Page in 2006 [2]. Since then, the pace of research efforts regarding alkali lasers have increased significantly, resulting in similar cesium (Cs) and potassium (K) laser demonstrations in 2003 and 2007 respectively [3, 4]. Subsequent efforts in improving all three of these systems have resulted in a kW-class Cs system with a conversion efficiency of 48% [5].

DPAL's have attracted the attention of the laser community for several reasons. Due to the small spectral spacing between the upper two levels of any 3 level DPAL, about 15 nm for Rb and 5 nm for Cs, these systems have quantum efficiencies of between 95 and 99%. This allows mixing between the upper two states via a buffer gas and reduces the total amount of waste heat produced in the gain medium. In addition, the fact that the gain medium is a vapor makes overall thermal management of the gain medium easier than in a solid state laser system.

When used in conjunction with a suitable diode laser, a DPAL can be used as an electrically driven system with no need for hazardous chemicals or complicated pump systems. In addition, due to their exceptionally high gain coefficients, orders of magnitude higher than that of other gas phase gain media, it is possible for a significant amount of power to be extracted from a small gain volume. These factors, combined with an exceptional beam quality due to the gaseous nature of the gain medium, result in a system that has come under investigation for use in high energy laser applications.

As part of this investigation, it is important to characterize atmospheric absorption in the near-IR region. For example, it is known that several water vapor absorption lines surround both the Cs and Rb DPAL emission lines. The spectral region around potassium (K), however, contains several strong oxygen (O₂) absorption features. These absorption features will affect a propagating laser beam based on their location with relation to the emission line as well as the strength of the absorption feature.

Due to the 20 nm tunable range of the diode heads used, it was possible to scan over the majority of the R-branch of the (0 0 0)→(0 0 3) H₂O vibrational band. By observing the width of two of the rotational lines in this branch, it was possible to investigate the rotational dependence of broadening rates. These values were then compared to broadened half widths reported in the HITRAN 2008 database.

Previous TDLAS investigations at DPAL wavelengths have been conducted at path lengths of 150 m and 1 km. By collecting absorption spectra for a 2 km path, it is possible to more accurately predict how a high energy laser (HEL) system using a DPAL would perform over longer distances. This comparison also allowed for an investigation of the dependence of absorbance on path length and concentration. Doubling the path

length allows for a better understanding of the difficulties associated with performing future TDLAS investigations at increased path lengths. In addition, this test was performed in a maritime environment, allowing for an investigation of how a higher concentration of water vapor affects the propagation of a DPAL. Characterizing the extent to which these absorption features degrade the performance of an alkali laser at longer path lengths and in different physical locations is an important step in determining the suitability of a system for various HEL applications.

II. Background

TDLAS Background

While conventional spectroscopy uses a broadband source and a resolving device such as spectrometer or interferometer to interrogate a sample, laser spectroscopy uses a spectrally narrow tunable laser. Through the use of a sufficiently narrow laser source, such as a dye laser or narrowed diode laser, it is possible to measure absorption features with a resolution limited by the linewidth of the atomic or molecular transition of interest. The introduction of tunable diode lasers makes laser spectroscopy much more convenient by cutting out the more traditional complex dye laser systems and replacing them with electrically driven systems. While they typically have lower output powers than dye lasers, tunable diode lasers offer a linewidth of less than 1 MHz and can typically be tuned over a range several nanometers. These performance characteristics, in addition to their reduced complexity and size compared to dye laser systems make TDLAS an excellent tool for investigating molecular absorption in the atmosphere with resolution limited by pressure broadening.

H₂O Spectroscopy

Because of its bent triatomic structure, a water molecule has three vibrational modes. The first, ν_1 , is referred to as a symmetric stretch. In this mode, both hydrogen atoms oscillate back and forth with respect to the oxygen atom symmetrically. The second, ν_2 , is referred to as a bend. In this mode, the molecule straightens out and flexes again. The third mode, ν_3 , is the asymmetric stretch. In this mode, one hydrogen moves

toward the oxygen molecule while the other moves away. These three modes make up the vibrational quantum number for H₂O and are typically represented as (v₁, v₂, v₃). [6]

A diagram of each of these modes is shown in Figure 1 below.

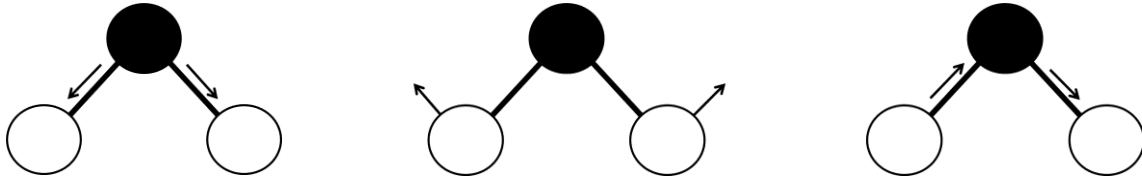


Figure 1: Three vibrational modes of a water molecule, the symmetric stretch (left), the bend (center), and the asymmetric stretch (right).

The rotational states within a vibrational band are represented in a similar way.

Because water is an asymmetric rotor, each rotational transition must be represented by three rotational quantum numbers, J, K_a, and K_c. The primary rotational quantum number, J, represents the total amount of rotational energy contained by the molecule, with K_a and K_c representing the two symmetric limits of the possible orientations of the hydrogen atoms with respect to the oxygen atom which taken together define how asymmetric the molecule is. These three quantum numbers are typically listed as [J, K_a, K_c], similar to the vibrational quantum numbers [6]. Using these two representations, it is possible to characterize a spectrum using the vibrational band and the rotational transition within that band.

Molecular Absorption

The primary principle at work in TDLAS is Beer's Law. Beer's Law relates the ratio of the intensity transmitted through a sample, I_t , and the incident intensity, I_0 , with

the absorption cross section, σ , species concentration, N , and path length, l as a function of the frequency in wavenumbers, $\tilde{\nu}$, by the relation

$$I_t(\tilde{\nu}) = I_0(\tilde{\nu})e^{-\sigma(\tilde{\nu}) \cdot N \cdot l} \quad (1)$$

with the absorption cross section given by the relation

$$\sigma(\tilde{\nu}) = \frac{g_2}{g_1} \frac{\lambda^2}{8\pi} A_{21} g(\tilde{\nu}) \quad (2)$$

where g_2 and g_1 and the degeneracies of the two states of interest, λ is the wavelength of the transition at the line center, $\tilde{\nu}$ is frequency of interest expressed in wavenumbers or inverse centimeters. A_{21} is the spontaneous emission coefficient, and $g(\tilde{\nu})$ is the lineshape function, taking the form of a Gaussian, Lorentzian, or Voigt profile. At times, it is more convenient to combine the absorption cross section with the species concentration in one variable, the absorption coefficient, $\alpha(\tilde{\nu})$ which can be used to rewrite Beer's Law as

$$I_t(\tilde{\nu}) = I_0(\tilde{\nu})e^{-\alpha(\tilde{\nu}) \cdot l}. \quad (3)$$

Lineshapes

The lineshape function, $g(\tilde{\nu})$, can have one of three forms. The first, the Lorentzian profile, takes the form

$$g_L(\tilde{\nu}) = \frac{\Delta\tilde{\nu}_L/(2\pi)}{\left(\frac{\Delta\tilde{\nu}_L}{2}\right)^2 + (\tilde{\nu} - \tilde{\nu}_0)^2} \quad (4)$$

where $\tilde{\nu}_0$ is the frequency at line center expressed in terms of wavenumbers and $\Delta\tilde{\nu}_L$ is the FWHM of the a Lorentzian profile in wavenumbers, given by

$$\Delta\tilde{\nu}_L = 2p_{\text{torr}} \sigma_{ik} \sqrt{\frac{2}{\pi \mu k T}}. \quad (5)$$

where p_{torr} is the pressure in torr, σ_{ik} is the collisional cross section for species of interest, μ is the reduced mass of the collision pair, k is the Boltzmann constant, and T is temperature in Kelvin. The lineshape takes this form in the case of homogenous pressure broadening, meaning that as you increase the pressure, the line will broaden regardless of its spectral relation, typically at a rate of around 10-20 MHz/torr. In the case of open path TDLAS, the pressure is around 1 atm, which equates to 760 torr. This results in a typical pressure broadened linewidth of ~10 GHz, much larger than the instrument limited resolution dictated by the laser source of ~300MHz.

The second form the lineshape function could take is that of a Gaussian, the form of which is given as

$$g_D(\tilde{\nu}) = \frac{2}{\Delta\tilde{\nu}_D} \sqrt{\frac{\ln(2)}{\pi}} e^{-4 \ln(2) \left(\frac{\tilde{\nu}-\tilde{\nu}_0}{\Delta\tilde{\nu}_D}\right)^2}. \quad (6)$$

where $\Delta\tilde{\nu}_D$ is the FWHM of a Doppler broadened lineshape, given as

$$\Delta\tilde{\nu}_D = 7.2 \times 10^{-7} \tilde{\nu}_0 \sqrt{\frac{T}{M}}. \quad (7)$$

where T is temperature in Kelvin and M is mass in atomic mass units. The Gaussian lineshape is found in the case of inhomogeneous broadening caused by an increase in temperature [7]. For typical values of temperature experienced over the course of this experiment of around 290 K, the FWHM is ~1 GHz, again larger than the instrument limited resolution. However, this is an order of magnitude below the pressure broadened FWHM, meaning that the primary factor governing the overall broadening rate of spectral lines is pressure.

While it is an order of magnitude higher than the Doppler broadened width, the pressure broadened FWHM is not sufficiently large to entirely dominate the overall FWHM. Because of this, it is important to also consider the temperature broadening rate when analyzing the overall lineshapes in the data collected over the course of this experiment. This is done through the use of a Voigt profile, a convolution of the relevant Lorentzian and Gaussian lineshapes. The HITRAN 1996 documentation provides a method for using parameters found in the HITRAN database to determine the half width of an absorption feature through the relation

$$\gamma(p, T) = \left(\frac{T_{ref}}{T}\right)^n (\gamma_{air}(p_{ref}, T_{ref})(p - p_s) + \gamma_{self}(p_{ref}, T_{ref})p_s). \quad (8)$$

where T and T_{ref} are the actual and reference temperatures in Kelvin, p , p_s , and p_{ref} are the actual pressure, partial pressure of the molecule of interest, and reference pressure in atmospheres, γ_{air} and γ_{self} are the air-broadened and self-broadened half widths found in the HITRAN database, and n is the exponent dictating the temperature dependence of the transition, also found in the HITRAN database. $\gamma(p, T)$ is the actual half width, corrected from the reported half widths to account for temperature and pressure [8].

The partial pressure of the molecule of interest, in this case water vapor, is found by multiplying the vapor pressure of water in the atmosphere by the relative humidity in the atmosphere. The vapor pressure was found using the relation

$$p_{vap} = \log_{10}(p_{st}) + 8.1328 \times 10^{-3} \left(10^{-3.49149(T_{st}/T-1)} - 1\right) + 10^{-7.90298(T_{st}/T-1)} + 5.02808 \log_{10} \left(\frac{T_{st}}{T}\right) - 1.3816 \times 10^{-7} \left(10^{11.344(1-T_{st}/T)}\right). \quad (9)$$

where p_{vap} is the vapor pressure in hPa, T_{st} is the vaporization temperature of water, T is the actual temperature, and p_{st} is the 1 atmosphere in hPa [9].

Water vapor exhibits over 250 absorption lines over the 890 nm to 910 nm range surrounding the Cs DPAL emission line. These lines are described by independent Voigt lineshapes, which are superimposed onto another on a frequency axis to form a complete spectrum. With information about precise transition frequencies and absorption coefficients for each of these independent lines and knowledge of the temperature, pressure, and concentration during an experiment, it is possible to use these relations to generate a spectral model with which to compare experimental results.

The reverse is also true. Using the Line By Line Radiative Transfer Model (LBLRTM) and the parameters found in the HITRAN database, it was possible to simultaneously fit a Voigt profile to each known spectral line in a collected data set using temperature, pressure, and concentration as variable parameters in order to obtain estimates for those variable parameters listed. In the absorption coefficient, the species concentration is found multiplied by the absorption cross section. This means that an increase in concentration will have the effect of increasing the strength of every absorption line in the spectrum by the same ratio. Atmospheric pressure is found within the Lorentzian contribution to the Voigt profile. As pressure increases, the lineshape will broaden, meaning that the majority of pressure information is contained in the wings of an absorption feature. Unlike concentration and pressure, temperature is determined not by Beer's Law parameters, but rather by the Boltzmann intensity distribution of the rotational energy levels in the absorption spectrum. As the temperature changes, the

rotational transition with the highest intensity will change. The peak rotational transition is found using the relation

$$J_{max} = \frac{1}{2} \sqrt{2kT/B_v} \quad (10)$$

where k is the Boltzmann constant, T is the temperature, and B_v is the rotational energy constant for a given vibrational transition. With a rotational constant of 435.346 GHz for water and an atmospheric temperature of 290 K, the calculated maximum rotational quantum number is 2.134. This compares favorably with the observed peak of ~ 2 . All other parameters which determine lineshape, such as species mass, line center location, and stimulated absorption coefficients are fixed values for a given species and will not change over the course of an experiment.

Molecular Scattering

In addition to molecular absorption, Rayleigh scattering also affects the way in which light propagates through the atmosphere. This is the scattering of incident light due to particles much smaller than the wavelength of that light, typically atoms or molecules. Rayleigh scattering has a λ^{-4} dependence, meaning that shorter wavelengths are scattered more than longer wavelengths. Because of this dependence, scattering introduces a baseline curvature of around 9% from 890 nm to 910 nm. This scattering is independent of absorption, meaning that it is possible for scattering to obscure absorption features if baseline noise is not the dominant effect. The scattering coefficient is typically on the order of 10^{-7} cm^{-1} , meaning that scattering effects alone can conceal absorption features lower than 10^{-2} in absorbance at a distance of 10^5 cm . This limit is an

order of magnitude lower than the observed noise in the baseline of the data collected at 2,000 m.

Turbulence

Atmospheric turbulence, when significant, can also degrade the performance of a laser at long propagation distances. The small changes in temperature along the path of the beam induce changes in the index of refraction, which bend and distort the beam as it travels. The resulting expanded effective diameter of the distorted beam a distance R away from the laser aperture is given by the relation

$$a_t = \frac{\sqrt{2}\lambda R}{\pi r_0}. \quad (11)$$

where a_t is the effective diameter, λ is wavelength, and r_0 is given by

$$r_0 = 3.02(C_n^2 R k^2)^{-\frac{3}{5}}. \quad (12)$$

where C_n^2 is a measure of turbulence related to the index of refraction and k is $2\pi/\lambda$ [10].

At the range and frequency of interest, the effective beam diameter was found to be ~ 5 cm. This equates to a turbulence induced jitter, defined as a_t/R , of ~ 50 μ rad. With a turning mirror diameter of ~ 15 cm, a total transmit telescope jitter of approximately 150 μ rad would be required to completely misalign the system. This means that while turbulence could contribute to noise in the baseline, it is not likely to cause a total misalignment of the system.

III. Equipment

The TDLAS device is composed of the tunable diode laser source, transmit and receive telescopes, and control and signal collection equipment. A mirror was included to return the transmitted beam to the receive telescope so that the transmit and receive telescopes did not have to be located at separate sites, easing data collection.

New Focus Velocity 6314 and 6318 lasers were used as the tunable diode sources depending on which alkali line was being investigated, 6314 being used for the Rb region and 6318 for Cs. Both of these systems are capable of producing a 10 mW beam with a spectral width of 300 kHz. The 6318 laser system has a full tunable range of 20 nm, from 890 to 910 nm. Fine tuning in 0.15 nm increments can be accomplished through the use of a piezo which allows for fine tuning of the cavity length. The 6314 laser system has a full range of 10 nm, from 790 to 800 nm, and a fine tuning range of approximately 0.1 nm.

An Optics for Research IO-5 optical diode was placed immediately after the laser head in order to prevent any retroreflection into the tunable laser cavity. After being reflected by a 92/8 2 μm pellicle beam splitter, a portion of the beam was sent to a High Finesse WSU-2 wavemeter. When used in combination with a SIOS SL-03 stabilized HeNe laser with an accuracy of 10 MHz for calibration, this device enabled frequency measurements accurate to better than 2 MHz.

The remainder of the beam was then modulated by a Thor Labs EO-AM-NR-C1 optical modulator at 100 kHz and the modulated beam was coupled to an RC Optical System (RCOS) Ritchey-Chrétien 12.5" telescope by way of a single mode optical fiber.

Another identical pellicle splitter was attached to the telescope between the output of the single mode fiber and the telescope itself in order to send a portion of the beam to a Thor Labs PDA 100A Si reference detector. The remainder of the beam was expanded to nearly fill the secondary mirror of the telescope through the use of an asymmetric lens with a focal length of 25 mm. The beam was then expanded by the telescope and transmitted across a distance of approximately 1 km before being reflected back by a 6" protected gold mirror with a surface of flatness of $\lambda/20$. The reflected beam was received by another RCOS 12.5" telescope and focused onto a second identical detector, resulting in a total open path of $2,032 \pm 2$ m. In some experiments, a Triad Technologies reference cell containing Cs or Rb with no buffer gas was placed in a heater block between the receive telescope and the receive detector. This enabled easy spectral location of the alkali D_1 doublet in the processed spectrum.

Both detectors were coupled to Stanford Research Systems SR-850 lock-in amplifiers capable of processing a signal modulated at up to 100 kHz and producing a 512 Hz processed signal. Lock-in time constants were usually set at 30 or 100 ms with a filter dropoff of around 6 dB/decade.

IV. Experiment

Physical Setup

Experimental equipment was set up in two locations separated from each other by $1,016 \pm 1$ m over the Upper Machodoc River as seen in Figure 2 below.

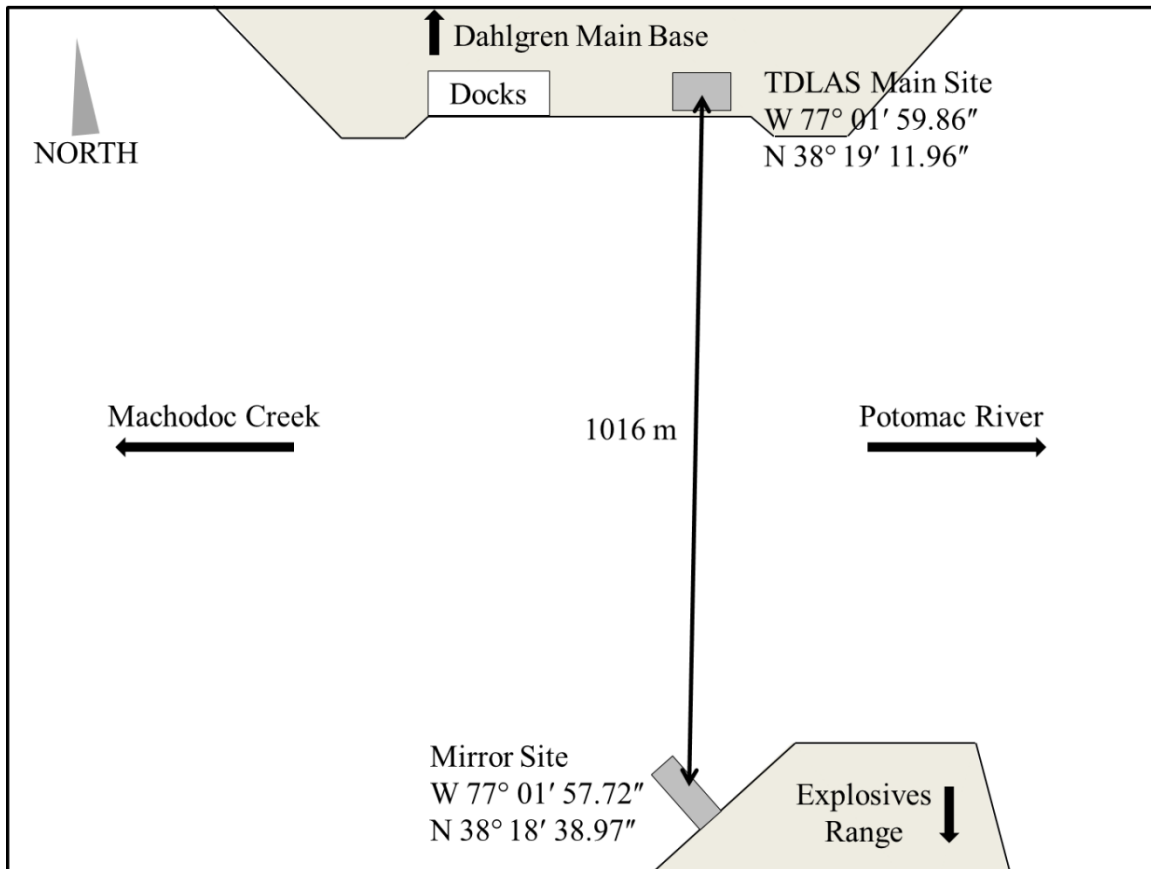


Figure 2: Diagram of the test site showing the TDLAS main site to the north and the mirror site to the south, separated by 1016 m. Exact coordinates for each site are shown. Machodoc River runs between the sites, beginning to the west and emptying into the Potomac River to the east.

The primary site was located on the north bank of the river at the southern tip of the Dahlgren Naval Surface Warfare Station. This site contained an Enterprise 16' commercial box truck on blocks, an 8' by 8' CONtainer EXpress(CONEX) military

shipping container, and a 10' by 10' tent, along with the receiver for the Scintec BLS900 scintillometer and the standalone Davis Vantage Pro2 weather station.

The box truck primarily functioned as a shelter and staging area for the Tunable Diode Laser Absorption Spectroscopy (TDLAS) device and testing equipment. The RC Optical System Ritchey-Chrétien 12.5" transmit and receive telescopes were placed on QuickSet QPT130 gimbals and tripods located just inside the rear opening of the truck, limiting any obstructions the beam would encounter. The tunable diode laser source and TDLAS control and signal collection equipment were placed on a cart deeper inside the truck. The truck was placed on blocks in order to minimize platform movement allowed by the suspension and tires, isolating the test equipment from as much of the vibration and movement caused by wind and human movement as possible. By doing this, the primary sources of platform jitter were limited to wind buffeting the telescopes and platform flex.

The CONEX, placed next to the truck, was originally intended for use as a temporary shelter for the TDLAS test equipment, however, it was instead used as a storage shelter for extra materials due to its small size and flexibility in the floor. The 10' by 10' tent was used as a remote shelter from which the telescopes could be aligned and the TDLAS equipment could be controlled without disturbing the box truck and the equipment inside. While the floor of the truck was sturdy, it was determined that the movement of a person from one end of the truck to the other or a person exiting the truck was sufficient to misalign the laser over a space of two kilometers. In addition, the tent housed the Kanomax handheld particle counter and its control laptop. This device was placed in the tent due to the need to routinely recharge the alcohol cartridge, an

action which could have disturbed the truck had it been placed with the rest of the equipment. The sample collection inlet was pointed toward the entrance to the tent, allowing for maximum exposure to outside air. A diagram and picture of the main test site are found below in Figures 3a and 3b.

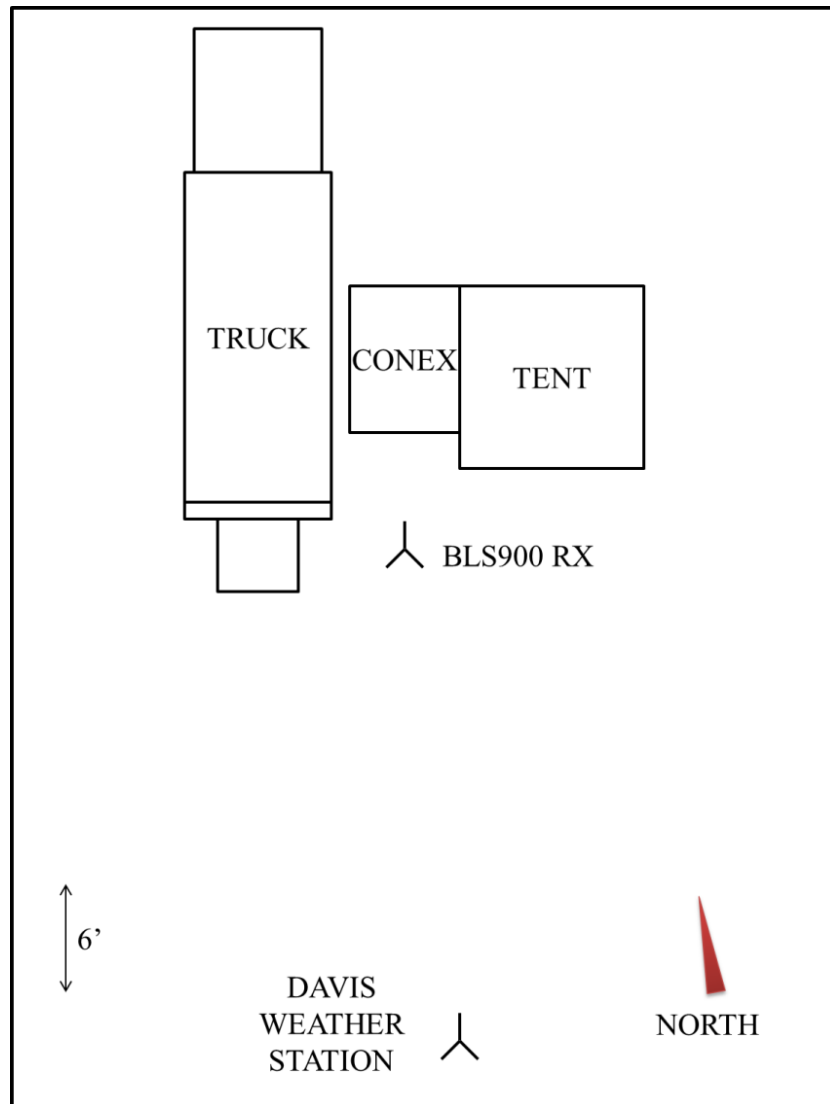


Figure 3a: Diagram of the TDLAS main site. The Dahlgren Naval Surface Warfare Center is located to the north and the river is to the south.



Figure 3b: Picture of the TDLAS main site showing the physical setup of the test equipment at the main test site. The control tent is on the left, the CONEX storage container is in the middle, and the box truck containing the majority of the test equipment is on the right. The BLS 900 Scintillometer receiver and processing unit are located in front of the CONEX.

The second site was located on a dock on the south side of the river on the north end of the Churchill explosives area. Here, a second 10' by 10' tent was used to shelter the turning mirror as well as the transmitter for the BLS900 scintillometer. By using permanent power located at the dock, it was possible to run the BLS transmitter for 24 hours a day for the duration of the test. In addition, a large 2' by 4' alignment target made with a large piece of rigid foam and reflective tape was placed on the dock in order to aid in location of the transmitted beam from the primary site one kilometer away. A diagram and a picture of the mirror site are shown in Figures 4a and 4b below.

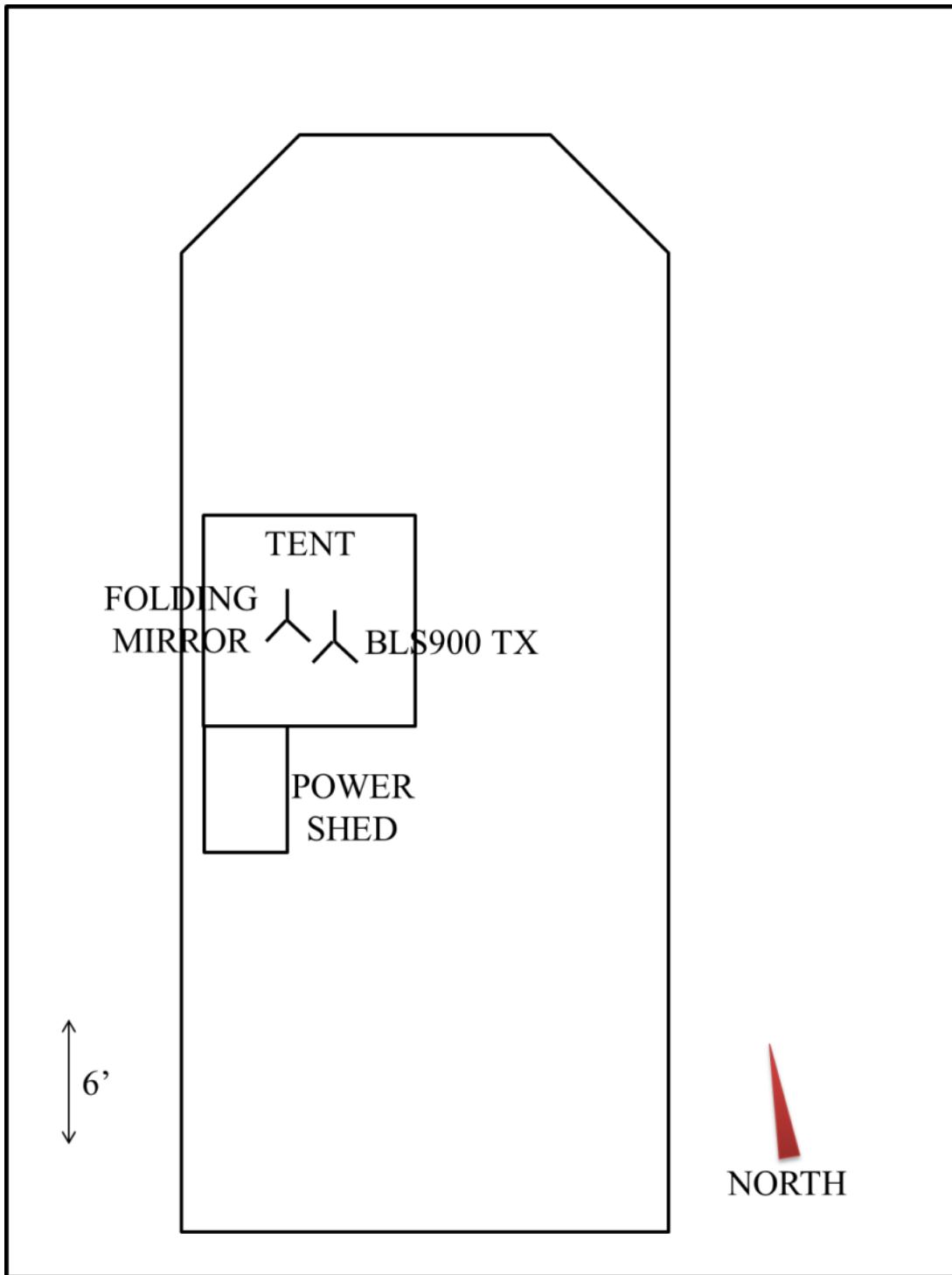


Figure 4a: Diagram of the mirror dock site. The dock extends into the river from the south



Figure 4b: A picture of the mirror site showing the physical layout of the test equipment. On the left is the BLS 900 Scintillometer transmitter, in the center is the 6" turning mirror, and on the right is a crude retro reflector array borrowed from Dahlgren NSWC. A large foam rectangle with reflective strips was taped to the shed behind the test equipment to aid in alignment.

Experimental Procedure

Before an experiment was run, it was important to ensure proper alignment of the TDLAS optical system, the telescopes, and the turning mirror. First, the power being coupled into the single mode fiber going to the telescope was maximized. This was accomplished by adjusting the location of the objective lens and the placement of the fiber relative to the lens until the maximum laser power possible was coupled to the single mode fiber.

Second, the placement of the single mode fiber coupled to the wavemeter was adjusted until the power reaching the wavemeter was allowed for an integration time of around 10 ms. This ensured that the laser power reaching the fiber was to be strong enough for the wavemeter to easily process, yet not so strong as to overwhelm the wavemeter detector.

In order to ease the alignment of the transmitted IR beam, a 5 mW visible alignment HeNe was mounted to the top of the transmit telescope. This was accomplished following the first successful alignment of the transmit and receive telescopes. Once the maximum possible signal was being reflected back to the receive telescope, the visible alignment laser was turned on and pointed at the center of the turning mirror. When the coalignment process was complete, the visible laser was reflected back towards the receive telescope, appearing 4 to 5 inches below the telescope aperture. This offset was due to the fact that the alignment laser was mounted above the transmitted beam, forcing the alignment beam to return below the received beam when both telescopes were perfectly aligned.

Coarse telescope alignment was accomplished with an individual in the back of the box truck. After coaligning the visible alignment HeNe with the transmitted TDLAS beam, alignment prior to an experiment primarily consisted of locating the alignment beam and translating the telescope such that it hit the mirror. At this point, the alignment beam was turned off and the transmit telescope was finely tuned to ensure maximum atmospheric transmission of the reflected beam. This was accomplished by viewing the mirror through the receive telescope with an IR viewfinder and finely adjusting the angle

of the transmitting telescope until the intensity returning to the receive telescope reached a maximum.

Coarse alignment of the receive telescope was accomplished by placing an opaque alignment disc at the image focus of the receive telescope and changing the angle of the telescope until the image of the mirror was centered on the disc. The disc was then replaced with a Triad Technologies reference cell containing the alkali of interest and detector and the receive telescope was finely adjusted to maximize the signal on the receive detector. The reference cell was heated to just above the melting point of the alkali of interest using cartridge heaters.

A similar method was also used to ensure proper alignment of the mirror. If mirror alignment was required, the angle of the mirror was changed until the image of the transmitting telescope aperture as viewed through the receive telescope was centered on the mirror.

Fine telescope alignment was then accomplished from the remote control tent. Because of the slight change in the vertical pointing angle caused by the weight of an individual in the truck, the transmit and receive telescopes were adjusted to point down slightly after the truck was empty, enabling the maximum signal to be collected by the receive telescope.

Atmospheric Absorption Spectra

From 17 October 2012 to 23 October 2012, full spectra were collected near the Rb and Cs D₁ emission lines. In the case of Cs, a New Focus Velocity 6318 was used as the tunable diode laser source. Two spectral ranges were investigated, one comprised of the entire tunable range of the diode and the other focusing on the range 5 nm on either

side of the Cs D₁ line. The wider range was typically conducted using a scan speed of approximately 0.005 nm per second with one or two averages per piezo range. These parameters were selected in order to keep collection times to below two hours. This time limit was imposed due to the difficulty in maintaining telescope alignment over 2 km for an extended period of time. Typically, telescopes stayed aligned for between 100 to 150 minutes. For the narrower spectral range, it was possible to fit the same time constraint while using a scan speed as low as 0.003 nm per second as well as a greater number of averages.

In the case of Rb, a New Focus Velocity 6314 was used as the laser source. This system has a full scanning range of from 790 to 802nm and a piezo scan range of about 0.15 nm. Because of the reduced full tunable range, the narrow range was selected to be only 2.5 nm on either side of the Rb D₁ line. Scan rates were the same as those used in the Cs case.

Long Term Single Frequency Baseline Monitoring

In order to quantify how the standard deviation of the baseline changed as a function of turbulence or scattering, a single frequency located away from atmospheric absorption features was monitored continuously for a period of one or two hours. Due to the lack of strong H₂O absorption features in its scan range, the New Focus 6314 diode laser was used in this experiment. The frequency selected for monitoring was 12599.34 cm⁻¹. Due to the long term nature of the experiment, data was saved to the hard drive every ten minutes to prevent the total loss of data during an experiment due to a system malfunctions such as software crashes or hardware misalignments.

Long Term Single Line Monitoring

In order to extract temperature and concentration as a function of time, two moderately strong rotational H₂O absorption lines were monitored over the course of an hour. These lines were chosen based on their strength and resolvability from other nearby lines. In order to avoid saturating the lock-ins, which can only reliably detect absorption to around 4, the selected lines were no greater than a 2 in absorbance. Based on these criteria, the lines located at 11192.69 and 11176.80 cm⁻¹ were selected for monitoring. The New Focus Velocity 6318 laser head was chosen for this experiment due to the presence of several strong H₂O lines in its operating range. In order to obtain data for both lines as near to each other in time as possible, each line was scanned for one minute, after which the laser would tune to the second line, scanning it for one minute before returning to the first line. This process was repeated up to 30 times, gathering pairs of lines that could be fit LBLRTM spectra generated using the HITRAN 2008 database in order to extract temperature and concentration estimates that could be compared with collected weather data

Meteorological Data

Turbulence data was collected by a BLS900 Boundary Layer Scintillometer. The transmitter, placed under the tent at the mirror site, was mounted on a tripod 1.2 m above the ground. In order to reliably obtain the maximum range of crosswind speeds, 0.1 to 30 m/s, the maximum possible pulse repetition rate of 125Hz was used. Permanent power at the mirror site allowed for collections to be taken for the entire duration of the test. The receiver, located at the main TDLAS site, was also placed on a tripod 1.2 m off the ground. The signal processing unit was placed on the ground next to the receiver tripod.

At 1016 m, the scintillometer was able to measure C_n^2 turbulence values between 4×10^{-15} and 4×10^{-11} . The integration time of the processing unit was set to the minimum allowed value of 1 minute in order to maximize the number of data points collected.

Particulate information was collected by a Kanomax handheld particle counter placed in the remote control tent. This device is capable of measuring particles concentrations of between 0 and 100,000 particles/cm³ for particles ranging in size from 0.015 to 1 μ m. This device was set to collect data once every five seconds in four hour spans. Typical particle counts were between 2,000 and 10,000 particles/cm³ with one instance of counts above 50,000 particles/cm³ corresponding to user actions around the counter.

Weather data was collected by a Davis Vantage Pro2 Weather Station set up at the main site. This station consists of a console unit placed inside the truck and a remote unit outside. This device collected continuous data for relative humidity, pressure, and temperature at 15 minute intervals with 95% confidence bounds of 6%, 2 hPa, and 1 C respectively.

Testing Schedule

15 October, Set Up, no collection (Started BLS Data Collection)

16 October, 1600-2100 – Cs Long Term Absorption Monitoring

17 October, 1500-2300 – Cs Spectra

18 October, 1100-1230 – Cs Spectra

19 October, 1300-2359 – Rb Spectra

20 October, 0000-0100 – Rb Spectra (continued from 19 Oct)

20/21 October, Data Analysis Days, No Collection

22 October, 1500-1830 – Rb Spectra

22 October, 1900-2100 – Cs Spectra

23 October, 1330-1700 – Rb Spectra

23 October, 1730-1930 – Rb Long Term Baseline

24 October, 1130-1930 – Rb Long Term Baseline

25 October, Pack, No Collection (Ended BLS Data Collection)

Table 1: Schedule showing what data was collected on each day of the test. Data was collected between 16 October and 25 October, with a day before and after this for set up and packing respectively. Cs and Rb Full represent days where full spectra were collected for each species. Cs Long represents a long term absorption line measurement and Rb Long represents a long term baseline monitoring collection.

Sun	Mon	Tuesday	Wed	Thur	Fri	Saturday
14 Oct	15 Oct	16 Oct	17 Oct	18 Oct	19 Oct	20 Oct
Travel Day	Set Up Day	1600-2100 Cs Long	1500-2300 Cs Full	1100-1230 Cs Full	1300-2359 Rb Full	0000-0130 Rb Full
21 Oct	22 Oct	23 Oct	24 Oct	25 Oct	26 Oct	27 Oct
Data Day	1500-1830 Rb Full 1900-2100 Cs Full	1330-1700 Rb Full 1730-1930 Rb Long	1130-1930 Rb Long	Pack Day	Travel Day	

V. Results

Meteorological Data

A BLS 900 Scintillometer was used to collect turbulence measurements for the 9 day duration of the experiment. At a range of 1,000 meters, the detectable range of C_n^2 values was 5×10^{-15} to 10^{-12} . A plot of the turbulence data for all 9 days as well as a sample from a single day are found in Figures 5a and 5b.

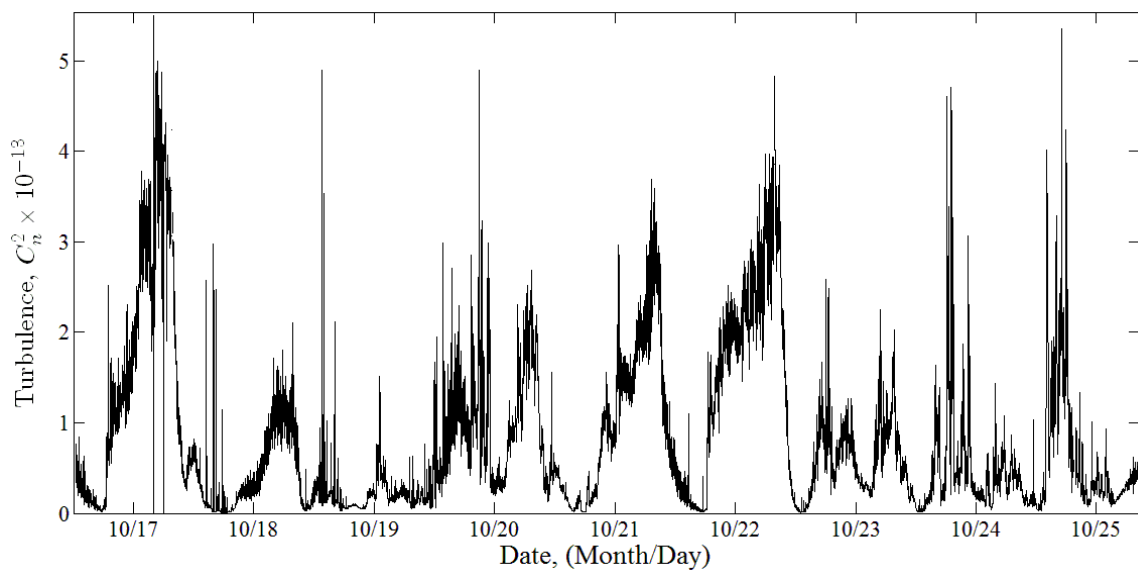


Figure 5a: C_n^2 measurements collected over the duration of the experiment. The turbulence values cycle from $\sim 5 \times 10^{-13}$ at night to $\sim 5 \times 10^{-15}$ in the afternoon just prior to sunset.

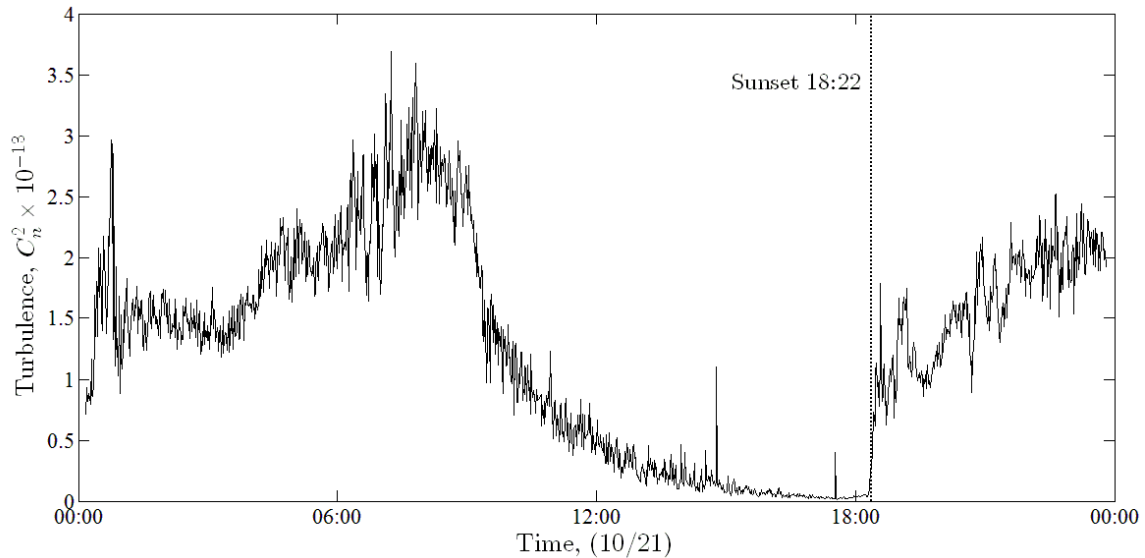


Figure 5b: Turbulence measurements for 21 October, highlighting the drastic rise in turbulence immediately following sunset.

Observed turbulence measurements ranged from $\sim 5 \times 10^{-15}$ to 10^{-12} , within the detectable range of the BLS 900 Scintillometer at 1,000 meters. The peak typically occurred in mid-morning, with C_n^2 values dropping through the afternoon to a low of approximately 10^{-14} just before sunset. The turbulence values consistently spiked by an order of magnitude immediately after sunset before slowly rising through the night and early morning to peak again in mid-morning. While turbulence on the order of that measured is not sufficient to misalign or completely degrade the propagating signal, it is possible that data taken during more turbulent periods could have a noisier baseline. Particulate counts were collected for several four hour time spans over the course of the experiment. The four hour limit is dictated by the length of time a single alcohol cartridge would function before having to be recharged. A sample of two of these scans

taken in quick succession on the afternoon of 22 October is shown in Figure 6 below.

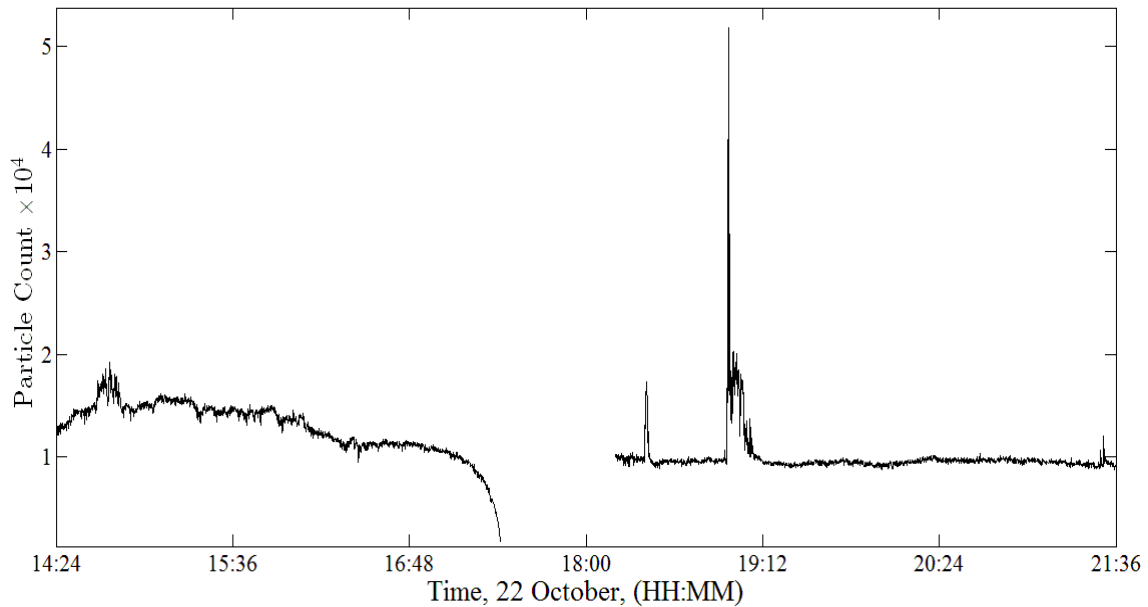


Figure 6: Particle counts for a seven hour block of time on 22 October 2012. This sample includes a count fall off around 17:15 corresponding to the alcohol cartridge in the particle counter failing as well as a spike of over 50,000 particles/cm³ corresponding to the spray of insect repellent near the collector inlet. Typical particle counts were on the order of 1,000 to 2,000 particles/cm³.

Typical particle values for the duration of the experiment were on the order of 10,000 to 20,000 particles/cm³. The maximum possible collection time was ~4 hours, at which point the alcohol cartridge must be removed from the counter and recharged for half an hour. The maximum value recorded was over 50,000 particles/cm³, which corresponds to a rapid influx of insect spray near the inlet of the particle counter. Several small peaks such as the one shortly after 1800 were observed and attributed to vehicle traffic around the test site.

Atmospheric Absorption Spectra

Broad Cesium Region Spectra

Data were collected for two spectral ranges, one consisting of the entire tunable range of the laser diode and another focused on the range around the DPAL D₁ emission line. In the Cs emission region, the maximum tunable range was from 890.5 to 909.9 nm, dictated by the tunable range of the laser diode used. An example of the spectrum collected over this range is found in Figure 7 below.

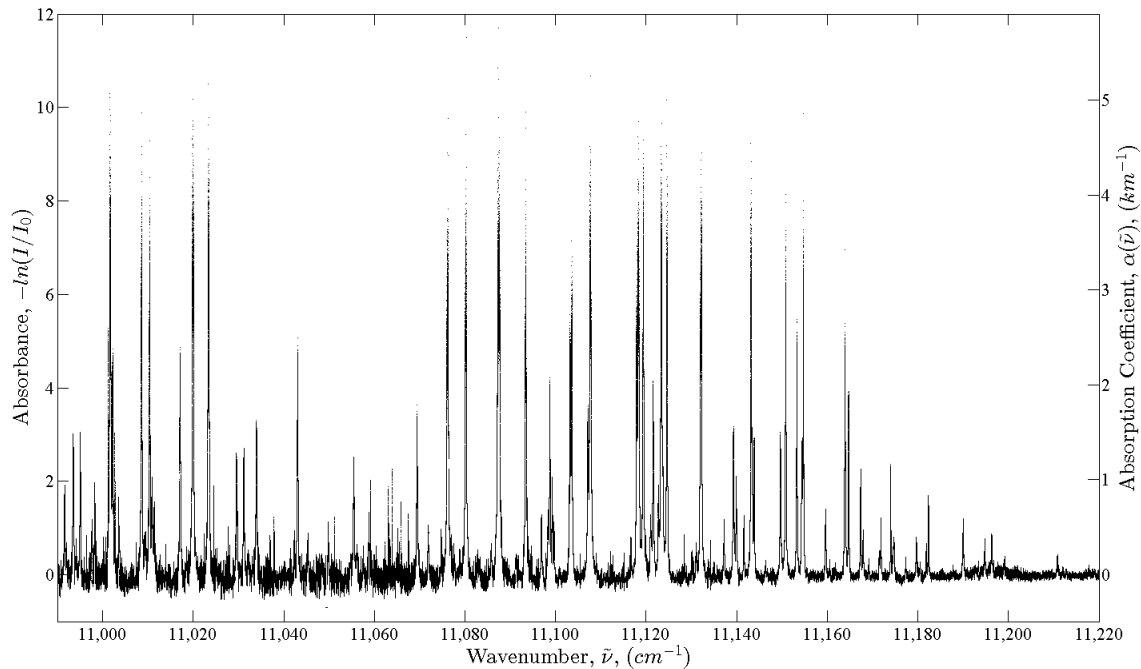


Figure 7: Atmospheric absorption spectrum of the entire 20 nm range of the New Focus Velocity 6318 Tunable Diode Laser. The majority of the spectrum is made up of the rotational structure of the (0 0 0)→(0 0 3) vibrational transition with some small contributions by the (000)→(102) transition.

This spectrum was collected at night, from 8:07 PM to 11:13 PM, on 18 October 2012 and is dominated by the R-branch of the (0 0 0) → (0 0 3) vibrational band of H₂O with rotational quantum numbers ranging from 0 to 10, the majority of which exhibit an

absorbance of 2 or greater at this distance. The P-branch and Q-branch have significant contributions at the lower energy end of the scan. Several weaker contributions by the $(0\ 0\ 0) \rightarrow (1\ 0\ 2)$ vibrational band of H_2O are scattered throughout the entire scan, all with an absorbance of less than 0.5. In total, over 250 absorption lines were identified in this spectrum. The locations of these lines, along with their relevant HITRAN data are listed in Table 4 of Appendix A.

The spectrum was fit to the known spectral lines in the HITRAN database using LBLRTM by varying the temperature, pressure, and concentration estimates until the residuals of a Voigt fit were minimized. The result was a temperature estimate of 282.6 ± 0.1 K, a pressure estimate of 0.9590 ± 0.0004 atm, and a concentration estimate of $3.2350 \pm 0.0009 \times 10^{17}$ cm^{-3} , with 95% confidence intervals on all three uncertainties. The standard deviation of the residuals of this final model fit is a measure of the noise in the baseline and determines the minimum detectable absorbance.

With a baseline noise of 0.14 and a maximum detected absorbance of 11.7, the signal to noise ratio (SNR) of this data set was calculated to be 83.6. Due to saturation of the lock-ins, this SNR is not entirely accurate. If instead the maximum detectable absorbance, 4, is used, the SNR becomes 28.6. With a maximum observed turbulence value of 3×10^{-14} , the turbulence induced jitter in this case was calculated to be 16 μrads . This is relatively low compared to the jitter induced by wind, which averaged 2.98 m/s over the course of this collection. While neither wind at this speed nor turbulence is sufficient to permanently misalign the system, the jitter induced by buffeting of the truck itself, the telescopes in the truck, and the folding mirror by the wind can induce significant noise levels into the data if it is not mitigated by signal averaging.

Narrowed Cesium Region

In one experiment, on 22 October 2012 at 7:05, a cell containing cesium at 34° C was included in the open path of the laser. This was done in order to easily identify the precise location of the cesium D₁ emission line at 894.6 nm. The full range of this scan was from 891.7 to 897.5 nm, approximately 3 nm on either side of the D₁ line. The 3.5 cm⁻¹ portion of this scan immediately surround the D₁ line is shown in Figure 8.

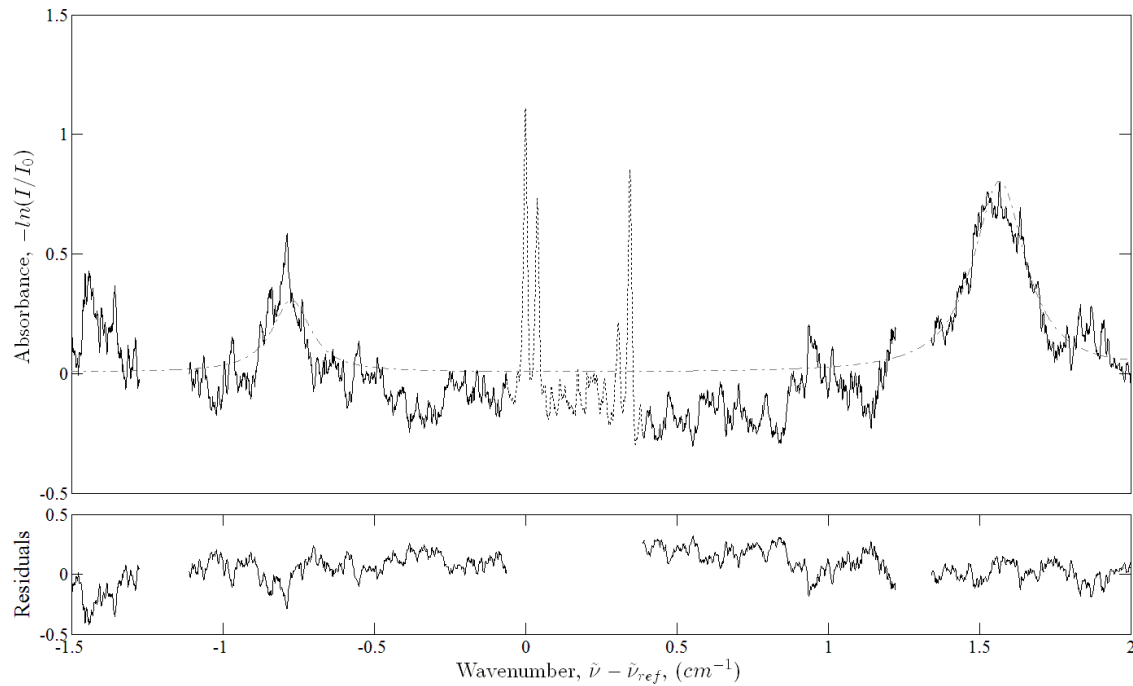


Figure 8: 0.3 nm sample of the atmospheric absorption spectrum collected over the 6 nm range immediately surrounding the Cs D₁ doublet. $\tilde{\nu}_{ref}$ is the energy of the lowest frequency line of the Cs doublet, 11178.112 cm⁻¹. The dashed line represents the LBLRTM fit to the collected data, displayed as black points. The Cs doublet appears as a dotted line and was excluded from the atmospheric model fit as Cs parameters are not included in atmospheric databases. The gaps in the spectrum are a product of the tunable laser failing to completely overlap consecutive scans.

The gray data points correspond to the Cs D₁ doublet. This data was excluded from the nonlinear fit because the HITRAN database does not include the Cs spectral

lines. With a standard deviation in the residual of 0.11 and a maximum detected absorbance of 8.4, the signal to noise ratio of this entire scan was calculated to be 76.4. Two H₂O absorption features are clearly visible on either side of the D₁ doublet, both corresponding to the rotational structure of the (0 0 0) → (0 0 3) vibrational transition. One line, corresponding to the [8 4 5] → [9 4 6] rotational transition, is located at 894.7 nm. The second feature is made up of two lines, one of which is due to the [9 5 5] → [10 5 6] rotational transition and the other of which is due to [6 2 4] → [7 2 5] rotational transition and is located at 894.45 nm.

Fit Correlations with Meteorological Data

Full absorption spectra were recorded throughout the 9 days of data collection, resulting in 6 data sets from which fit estimates for temperature, pressure and concentration could be extracted. In addition, the Davis Vantage Pro2 weather station recorded temperature and pressure for the duration of the test. The temperature, pressure, dew point, and relative humidity provided by the Davis weather station were used to obtain concentration measurements for the duration of the test. Figures 9a and 9b below show how the fit estimates compare to the measured temperature and pressure values respectively.

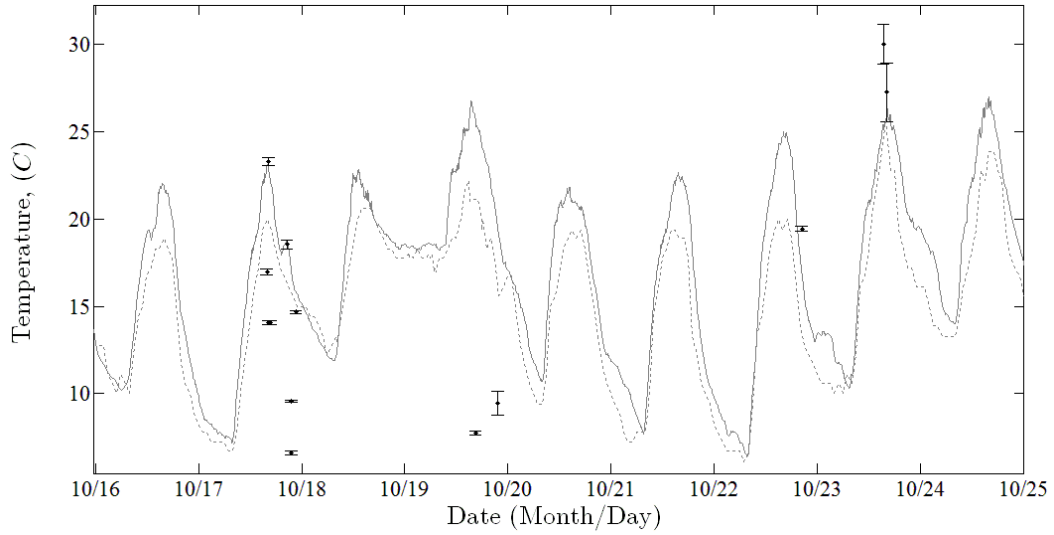


Figure 9a: Temperature measurements from the Davis Vantage Pro2 weather station (dark grey line), national weather station in Quantico, VA (dashed line), and spectral fit estimates (data markers) for the 9 day duration of data collection.

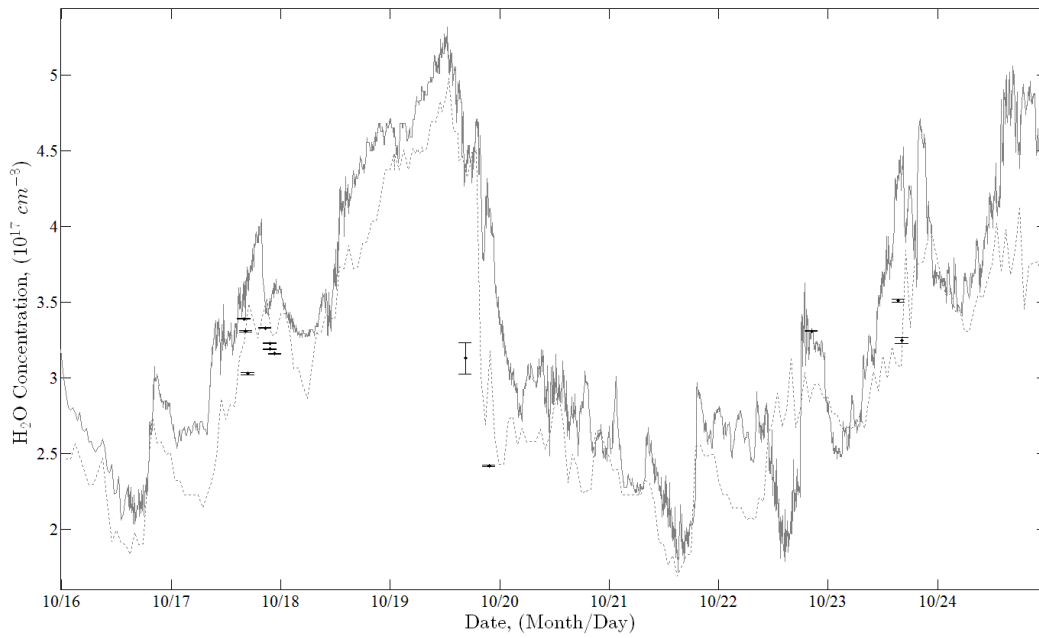


Figure 9b: Temperature measurements from the Davis Vantage Pro2 weather station (dark grey line), national weather station in Quantico, VA (dashed line), and spectral fit estimates (data markers) for the 9 day duration of data collection.

The data sets used in these fit estimates come from two collections on the evening of 17 October, two on the evening of 19 October, one on the evening of 22 October, and one from 23 October. Because of the broad spectral region scanned on 17 October, each of these scans was broken up into 3 parts and each region was fitted, providing three more data points per scan. This process was also applied at the test on the 23rd.

The temperature estimates from the experimental fits vary more widely and faster than the Davis weather station measurements with estimates in the evening of 18 October dropping at a higher rate, 3.18 degrees per hour, and ending at a lower temperature, 6.6° C, than the weather measurements at 0.73 degrees/hour and 11.9° C respectively.

Overall, temperature estimates ranged from 6.60° to 30.03° C while the Davis weather station reported values between 6.45° and 26.75° C, with an agreement of better than 6%.

In two cases, it was possible to divide the collected spectrum into 3 pieces which were then fit to LBLRTM independently. One of these scans, taken on 17 October, took place over a steep drop in temperature, allowing for a comparison estimates with the Davis weather station on a faster time scale. The estimates and errors for these three pieces as well as the entire scan are shown in Figure 10 below.

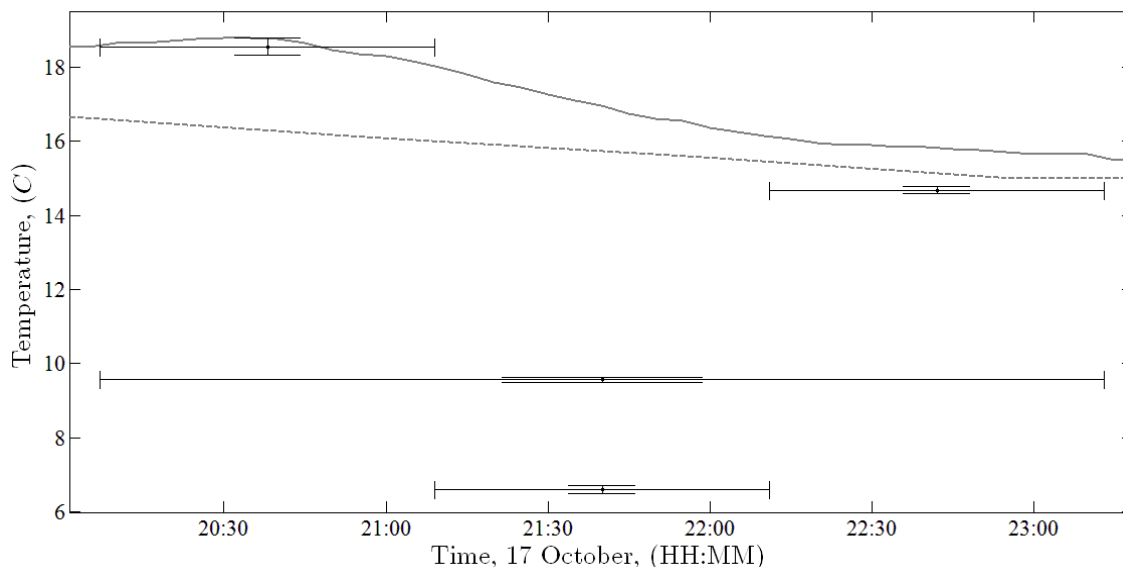


Figure 10: Fit estimates and weather station data for temperature on 17 October 2012. Vertical error bars correspond to 95% statistical errors from the fits and horizontal error bars represent the period of time covered by each piece of the collection. The solid grey line represents the Davis weather station data and the dashed line represents the temperature data from the national weather station at Quantico.

Concentration estimates for all of the analyzed scans ranged from 2.55×10^{17} and $3.5 \times 10^{17} \text{ cm}^{-3}$ with individual values being between 1 and 25% lower than calculated values which ranged from 1.79×10^{17} to $5.32 \times 10^{17} \text{ cm}^{-3}$. The estimates which were furthest from the calculated values were largest at times when the concentration was changing most rapidly. This discrepancy is likely due to the Davis weather station being placed several meters away from the edge of the river. Because the TDLAS laser is interrogating air over the river, it is possible that the both the absolute concentration and the rate at which that concentration changes as measured by the TDLAS device could differ from the value calculated by the meteorological data. In times of more stable concentrations, the discrepancy was reduced to between 1 and 10%. A summary of the

temperature and concentration estimates for each of the scans plotted is found in Table 2 below. In addition, plots of all data sets used to obtain these estimates are found in Appendix B.

Table 2: Scan times, fit estimates, 95% confidence bounds (\pm), Davis weather station, and percent error for each scan analyzed.

Date	Time		Concentration (10^{17} cm^{-3})				Temperature (K)			
	Start	End	Fit	\pm	Davis	Error	Fit	\pm	Davis	Error
10/17	15:45	16:10	3.39	0.01	3.64	7.37	289.95	0.17	296.1	2.12
10/17	16:10	16:35	3.31	0.01	3.54	6.95	296.29	0.24	295.75	0.18
10/17	16:35	16:59	3.03	0.01	3.6	18.81	287.09	0.11	295.15	2.81
10/17	20:07	23:12	3.23	0.01	3.53	9.29	282.57	0.07	289.95	2.61
10/17	20:07	21:09	3.33	0.01	3.42	2.70	291.55	0.24	291.75	0.07
10/17	21:09	22:11	3.19	0.01	3.53	10.66	279.6	0.11	289.95	3.70
10/17	22:11	23:12	3.16	0.01	3.63	14.87	287.68	0.09	288.85	0.41
10/19	16:28	19:09	3.13	0.11	4.42	41.20	280.74	0.13	298.65	6.36
10/19	21:59	00:48	2.42	0.01	4.09	69.01	282.45	0.67	292.25	3.47
10/22	19:05	21:56	3.31	0.01	3.33	0.60	292.44	0.14	280.05	4.24
10/23	15:05	15:42	3.51	0.01	4.33	23.36	303.02	1.14	299.4	1.19
10/23	15:51	16:28	3.25	0.02	4.39	35.08	300.27	1.68	298.45	0.61

Comparison with Previous Work

Recent research has been performed using the same TDLAS device used in this experiment to investigate Cs and Rb emission regions [11-15]. These experiments were performed at 150 m indoors and at 1 km outdoors on the Air Force Institute of Technology (AFIT) Laser Range. This previous work was able to use extensive signal averaging to drive the signal to noise ratio higher than 1,000. Such a high ratio is important in the accurate estimation of temperature, pressure, and concentration. Figure 11 below shows a spectrum collected at 2,000 m along with these previous spectra, collected at 150 and 1,000 m.

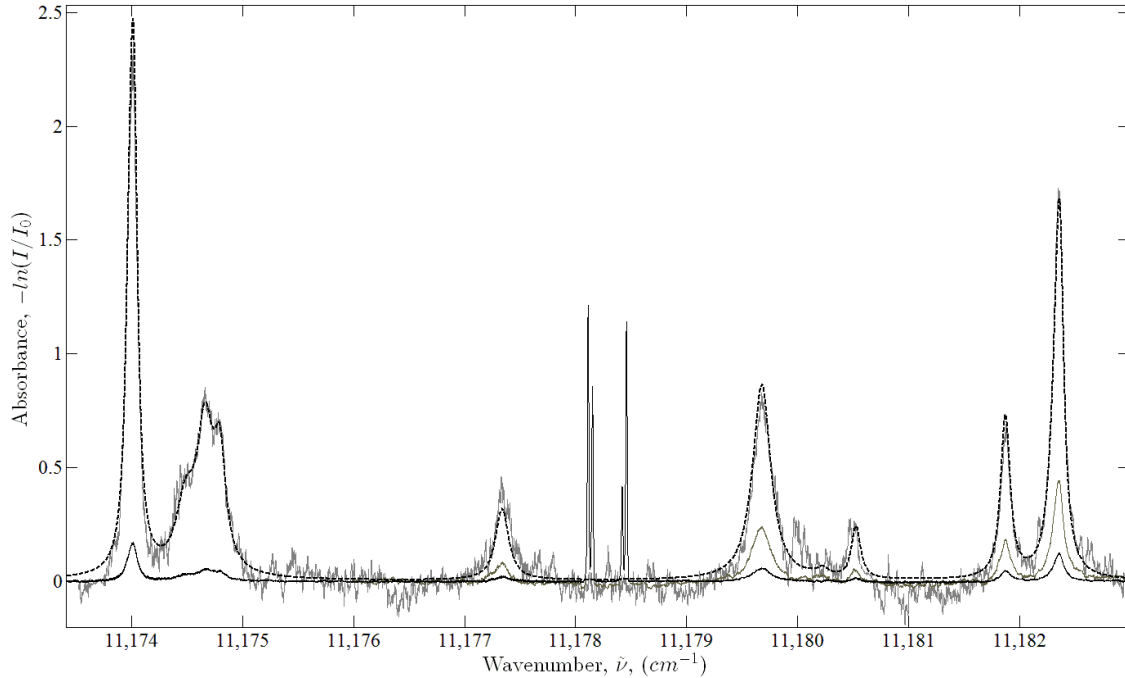


Figure 11: Atmospheric absorption spectra collected over the Cs D₁ spectral region at 150 m (black), 1,000 m (dark gray), and 2,000 m (light gray). The D₁ doublet is included in the spectrum collected at 150 m. The increase in baseline noise is clear as the experimental path length is increased, with a dramatic rise going to 2,000 m due to a lack of signal averaging as well as additional platform jitter.

The noise in the spectrum collected at the 2,000 meter path length is significantly higher than that at either previous distance. There are several reasons for this degradation. First, the wind speeds for this collection were around 3 m/s. This can induce jitter in the mirror as well as in the platform the telescopes were on. At around 50 μ rad, turbulence jitter could have also contributed to the degradation of the baseline, introducing noise without misaligning the system.

Further, by observing the intensity of the line at 11182.5 cm^{-1} at each range, 1.73, 0.44, and 0.12 at 2 km, 1 km, and 150 m respectively, it is seen that the strength of the line at 2 km is 3.9 times that of the 1 km distance. In addition, the intensity at 2 km is

13.3 times that at the 150 m case. Because of Beer's Law, it is known that absorbance is linearly related with both path length and concentration. Because absorption varies linearly with concentration, it is likely that the concentration of water molecules at Dahlgren, VA in October is roughly twice that at AFIT in winter, the location and date of the 1 km experiment. The intensity ratio between the 150 m and 2 km lines, however, is only slightly higher than the ratio of the distances, meaning the H₂O concentrations were likely similar during those tests.

These observations are consistent with concentration measurements taken at all three test sites. For the 150 m path length, a concentration of $3.096 \pm 0.004 \times 10^{17}$ molecules/cm³ was recorded. A concentration of $1.94 \pm 0.004 \times 10^{17}$ molecules/cm³ was reported for the 1 km path length. A concentration estimate of $3.23 \pm 0.001 \times 10^{17}$ molecules/cm³ was extracted from the data at the time of the 2 km test. The small increase in concentration at the 2 km test with respect to the 150 m test makes up the small discrepancy seen in the intensity ratio. The distance ratio multiplied by the concentration ratio between the two tests returns a total expected ratio of 13.9, only 3.4% below the observed value. In the case of the 1 km test, the total calculated ratio was 3.33, 15% below the observed intensity ratio. The remaining discrepancies in intensity are likely due to other meteorological parameters, specifically temperature. The temperature reported by the Davis weather station reported a value of 16.9 C, slightly higher than the 15 C reported for the 150 m case and significantly higher than the 6 C reported for the 1 km case. A summary of the concentration, path length, and absorption ratios can be found in Table 3 below.

Table 3: Observed concentration and absorption values for 150, 1,000, and 2,000 meter collections. All ratios are with respect to the relevant values at 2,000 meters. The ratio product is determined by multiplying the path ratio by the concentration ratio.

Length (m)	[H₂O] (x 10¹⁷ cm⁻³)	Observed Absorption	Path Ratio	[H₂O] Ratio	Ratio Product	Intensity Ratio	Error
150	3.096	0.12	0.075	0.932	0.0699	0.0694	0.73
1,000	1.940	0.44	0.500	0.601	0.3003	0.2543	18.07
2,000	3.230	1.73	1	1	1	1	0

Rotational Dependence of Broadening Rates

HITRAN lists values for air and self-broadened half widths as well as a method by which to correct these values to report an actual observed half width [16]. There is a slight change in the broadening coefficient that corresponds with a change in the rotational transition being observed. By finding two widely separated rotational lines in the same vibrational transition, it was possible to investigate whether or not it was possible to observe this change in the data collected at Dahlgren. The two lines selected were corrected to be centered at zero wavenumbers and normalized such that the peak absorbance was 1, as seen in Figure 12 below.

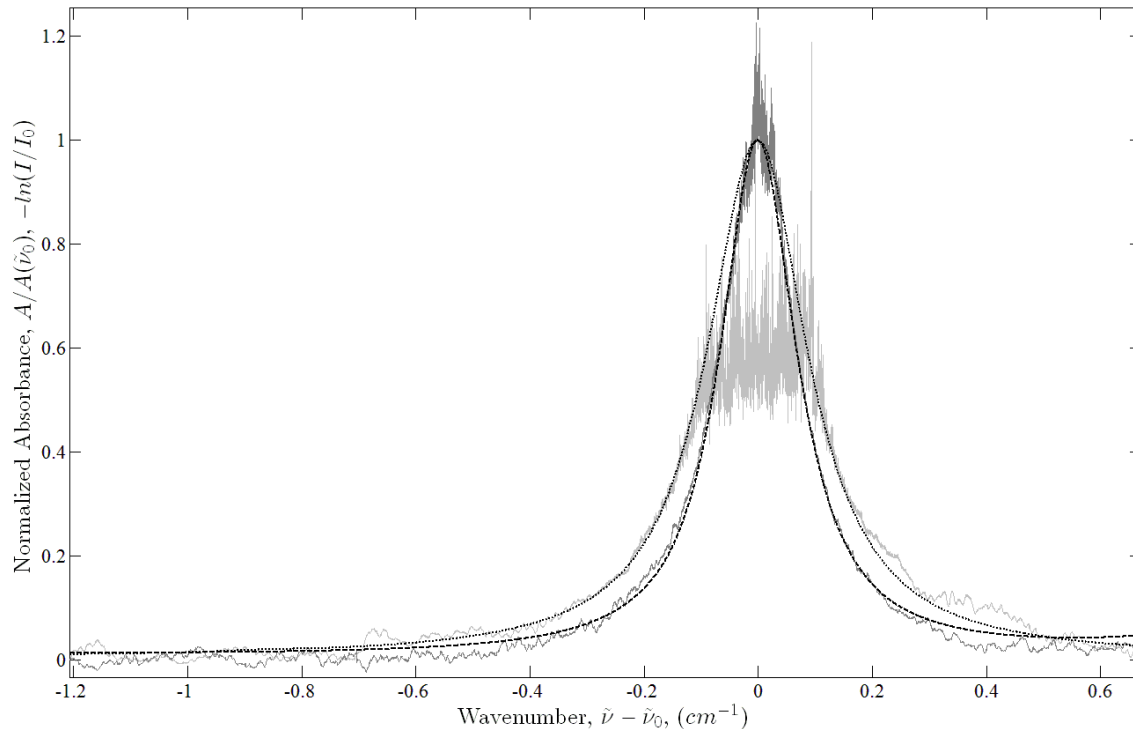


Figure 12: Absorption lines corresponding to the [1 1 0] \rightarrow [2 1 1] (light gray) and [6 2 5] \rightarrow [7 2 6] (dark gray) rotational transitions within the vibrational (0 0 0) \rightarrow (0 0 3) band, overlaid and normalized to a peak intensity of 1. An LBLRTM fit for each line is superimposed on the data, with the dotted line corresponding to the J = 2 line and the dashed line corresponding to the J =7 line. Noise in the top of each data set is due to absorbance beyond the detectable limit of the lock-in amplifiers.

Based on this plot, it was determined that the half width of the J=2 rotational line was 0.11 cm^{-1} . HITRAN reports this width as 0.082 cm^{-1} , leaving a discrepancy between the reported value and the experimental value 24%. The J=7 rotational line had a width of 0.08 cm^{-1} 28% higher than the value reported in HITRAN, 0.059 cm^{-1} . It is likely that the large discrepancy between the observed and theoretical values stems from the noise in the data. Because the determination of pressure, and thus linewidth, is so dependent on the wings of each absorption feature, there is a relatively large amount of uncertainty induced by noise in the data.

HITRAN lists the uncertainties in the reported values for the air-broadened half-width as being between 5 and 10%. The values reported for the self-broadened half width are listed as being either an average of multiple experimental results or as a best estimate, with an unknown amount of error. In addition, the amount of noise present in the experimentally collected 2 km data increases the error inherent in the nonlinear fit as well as complicating the determination of the half width from the data itself, with the range of frequencies corresponding to a normalized intensity of 0.5 being approximately 0.015 cm^{-1} . Despite the error in the broadening rates themselves, the ratio of the broadening rates at the J=2 line to the line at J=7 is 1.313 as determined by the fit values, only 5% below the ratio of the values reported in HITRAN.

VI. Conclusions and Recommendations

Conclusions of Research

A ruggedized TDLAS device has been deployed to Dahlgren, VA to investigate atmospheric absorption at DPAL wavelengths in a maritime environment at a path length of 2 km. Over the course of 9 days, experiments were conducted to investigate absorption around the DPAL emission lines of Rb and Cs, the way in which changing water vapor concentrations can affect the strength of absorption features, and the effects of various parameters on the noise in the baseline as well as the value of the baseline itself. This series of experiments showed the feasibility of later investigations at still longer path lengths as well as highlight some of the challenges that would accompany such an effort. In addition, performing this investigation at a longer path length showed how absorption features grow and broaden as the propagation distance grows. This information is valuable in determining how molecular absorption will affect a propagating laser beam.

Spectra were collected within the 20 nm range surrounding the Cs D₁ laser emission line as well as in a 10 nm range around the Rb D₁ line. With a maximum detectable absorbance of around 4 and a baseline noise level of around 0.1, the SNR for the spectral region surrounding Cs was limited to 40. With a lower peak detected absorbance due to the relative strength of the H₂O absorption lines, the Rb spectral region typically had a SNR of around 10. These values are significantly lower than those from previous efforts using the same device, as high as 1,000, due to the extended path length, increased platform jitter, and the lack of signal averaging. Temperature and

concentration estimates were made by fitting the collected spectra to the HITRAN database using LBLRTM. These estimates were used in conjunction with collected weather data to investigate potential differences in the ways temperature and concentration change over time over land and water. Temperature estimates, which ranged from 6.6° C at night to 30.02° C in the mid-afternoon, were within 6% of the corresponding values reported by a Davis Vantage Pro2 weather station, which ranged from 6.5° to 26.8° C. In addition, some differences in the rate at which the temperature changed over water as opposed to on land were noted, with the air over the water appearing to cool around 4 times faster than the air over the land. Concentration estimates were within 25% of the values calculated from the collected meteorological data, with the largest difference being found at points in time when the concentration was changing most drastically. Concentration estimates ranged from 2.55×10^{17} and $3.5 \times 10^{17} \text{ cm}^{-3}$ with calculated values for the entire 9 day period of data collection ranging from 1.79×10^{17} to $5.32 \times 10^{17} \text{ cm}^{-3}$.

Spectral and meteorological data from this 2 km investigation were compared to data collected at path lengths of 150 m and 1 km. By overlaying the collected spectra, it was possible to directly observe how the absorption features change as a function of path length and H₂O concentration. Because the water vapor concentrations were similar, on the order of $3 \times 10^{17} \text{ molecules/cm}^3$, between the 150 m and the 2 km tests, the relative strength of these absorption features was dictated primarily by the change in path length. Because the concentration at the 1,000 m test was roughly half that at the other tests, the relative strength of the absorption features was dictated in part by the change in path length and in part due to the change in species concentration.

By analyzing the linewidths of two rotational lines, the $[1\ 1\ 0] \rightarrow [2\ 1\ 1]$ transition at 11080 cm^{-1} and the $[6\ 2\ 5] \rightarrow [7\ 2\ 6]$ transition at 11153 cm^{-1} , from the $(0\ 0\ 0)$ to $(0\ 0\ 3)$ vibrational band, it was possible to investigate the rotational dependence of broadening rates. These broadened linewidths, as well as the ratio by which the broadening rate changes as a function of rotational quantum number, were compared to the values reported in the HITRAN database for the given transitions. The broadening rates from the two investigated lines were found to be 0.109 cm^{-1} for the lower line and 0.083 cm^{-1} for the upper line, both of which are between 25 and 30% higher than those reported by the HITRAN database, 0.0823 and 0.0594 cm^{-1} respectively. Despite this discrepancy, the ratio by which the broadening rate decreases as a function of rotational quantum number in the collected data is within 5% of ratio of the values found in the database.

Recommendations for Future Research

Continuous upgrades to the TDLAS device used in this experiment have allowed for a gradual increase in its utility. By upgrading the tunable diode laser system, the mirror, and the signal collection and processing equipment, the capabilities of the AFIT TDLAS apparatus will continue to increase dramatically.

In terms of the tunable diode laser system used to prepare the beam prior to expansion, replacing the free space system currently used with a fiber coupled scheme would have several benefits. First, it would drastically cut down on the amount of time required to change diode laser heads, increasing the efficiency of future experiments. In its current configuration, the changing of a laser head alone takes 15-30 minutes, with a

full alignment of all optics taking several hours. Considering the deployable nature of this system, a fiber coupled scheme would reduce or eliminate the risks associated with misalignment of the optical board as well as the time required to change the alkali being investigated.

In addition, while the visible alignment laser was effectively upgraded prior to this experiment to enable propagation over 2 km, efforts at longer distances would likely benefit from a new configuration. By coupling the visible alignment laser beam to the telescope itself such that the beam came from the same telescope as the TDLAS beam, it would be possible to quickly guarantee alignment over longer distances. In addition, it would decrease the time required to coalign the visible and IR beams, a task that must be accomplished at every new distance due to the current placement of the visible HeNe on top of the transmit telescope.

Several issues with regards to platform jitter were noted at the 2 km range of this test. With a baseline noise value anywhere from 0.1 to 1 in absorbance at 2 km, it is clear that future experiments at greater path lengths will require a significant reduction in the effects of platform jitter. One method currently being investigated is the use of a 1' by 1' retroreflecting array as a replacement for the 6 inch mirror currently being used. First, the increased area of the array means a larger effective target for the transmitted beam, reducing the impact of telescope jitter. Also, due to the nature of a retroreflector, all light incident on it will be returned along its initial trajectory, in this case back to the transmitting telescope. This property would significantly decrease the influence of mirror misalignment and jitter.

In terms of application, given the necessary upgrades, similar experiments to this one could be conducted at even greater distances, stretching beyond 5 km. Such efforts would be valuable in continuing to evaluate the performance of alkali laser wavelengths in the atmosphere. In addition, conducting similar tests in a growing number of locations would enable the characterization of the various alkali systems in the environments in which they would be used. By further increasing the path length interrogated and conducting experiments in various locations, it would be possible to more accurately gauge the performance of each alkali system in a given high energy laser scenario.

Beyond the investigation of DPAL wavelengths in the atmosphere, the broad range of rotational lines interrogated over the course of a full tunable diode laser scan provides an opportunity to investigate and validate the broadening rates listed in the HITRAN database. While this possibility was investigated, cleaner data would likely provide a much better estimate as to the observed broadening rate of each rotational line. In this way, the rotational dependence of the broadening rates found in HITRAN could be investigated with greater accuracy.

Long term baseline data was collected over the course of this experiment which could be used to further investigate the influence of turbulence and wind speed on baseline fluctuations. This data could be used in order to determine whether or not turbulence and scintillometry data could potentially be extracted from the baseline data of the spectra collected in these experiments.

Appendix A

Table 4: HITRAN 08 data for the lines observed in the 890 to 910 nm range surrounding the Cs D1 emission line.

Wavenumber (cm^{-1})	Intensity (cm/mol)	A_{21} ($1/\text{s}$)	Broadening		Temperature Coefficient	Lower						Upper					
			Self	Air		v_1	v_2	v_3	J	K_a	K_c	v_1	v_2	v_3	J	K_a	K_c
10991.6347	8.58E-24	4.91E-02	0.086	0.48	0.62	0	0	0	5	3	2	0	0	3	5	3	3
10992.0194	2.58E-24	7.36E-03	0.088	0.45	0.68	0	0	0	5	1	4	1	0	2	6	2	5
10993.2147	1.78E-25	2.63E-04	0.1	0.4	0.79	0	0	0	3	0	3	1	0	2	3	3	0
10993.4974	1.02E-23	1.80E-02	0.104	0.58	0.76	0	0	0	3	1	2	0	0	3	3	1	3
10993.5537	4.30E-24	1.90E-02	0.094	0.45	0.74	0	0	0	2	2	0	1	0	2	3	3	1
10995.0781	1.26E-23	1.85E-02	0.088	0.53	0.71	0	0	0	2	2	1	1	0	2	3	3	0
10996.2557	1.84E-25	5.42E-03	0.066	0.3	0.25	0	0	0	7	2	6	1	0	2	8	1	7
10997.5364	4.63E-25	6.90E-03	0.08	0.36	0.57	0	0	0	6	1	5	1	0	2	7	2	6
10997.683	4.14E-24	3.41E-02	0.097	0.48	0.73	0	0	0	4	2	2	0	0	3	4	2	3
10997.9416	3.82E-26	2.11E-02	0.073	0.28	0.45	0	0	0	10	4	7	0	0	3	10	4	6
10998.289	7.11E-24	8.15E-02	0.085	0.46	0.62	0	0	0	4	3	1	0	0	3	4	3	2
10999.458	6.32E-26	6.59E-04	0.043	0.33	-0.02	0	0	0	8	1	8	1	0	2	9	0	9
11000.1092	9.58E-26	7.62E-04	0.088	0.43	0.75	0	0	0	5	4	1	0	0	3	6	2	4
11001.6679	2.19E-23	8.32E-02	0.08	0.44	0.67	0	0	0	4	3	2	0	0	3	4	3	1
11001.7003	4.75E-23	1.45E-01	0.081	0.47	0.62	0	0	0	3	3	0	0	0	3	3	3	1
11002.2178	1.57E-23	1.44E-01	0.083	0.49	0.63	0	0	0	3	3	1	0	0	3	3	3	0
11002.7759	7.84E-26	4.09E-04	0.096	0.52	0.77	0	0	0	4	0	4	1	0	2	4	3	1

11003.4843	6.42E-25	6.17E-03	0.073	0.4	0.39	0	0	0	7	1	6	1	0	2	8	2	7
11003.6068	2.73E-24	4.59E-02	0.09	0.44	0.71	0	0	0	5	3	3	0	0	3	5	3	2
11005.9389	1.39E-25	5.19E-03	0.073	0.27	0.47	0	0	0	8	3	6	1	0	2	9	2	7
11006.1535	2.98E-25	6.19E-03	0.056	0.26	0.1	0	0	0	8	2	7	1	0	2	9	1	8
11007.5533	6.54E-27	2.16E-03	0.082	0.33	0.49	0	0	0	8	3	5	0	0	3	9	1	8
11007.651	8.23E-27	9.68E-05	0.099	0.44	0.73	0	0	0	4	0	4	0	0	3	3	2	1
11008.6106	3.16E-23	1.89E-01	0.104	0.44	0.73	0	0	0	1	0	1	0	0	3	0	0	0
11009.5155	2.88E-24	2.77E-02	0.09	0.46	0.74	0	0	0	6	3	4	0	0	3	6	3	3
11010.3822	2.79E-23	5.96E-02	0.095	0.47	0.74	0	0	0	3	2	1	0	0	3	3	2	2
11010.9303	7.48E-24	1.24E-02	0.093	0.47	0.79	0	0	0	3	2	1	1	0	2	4	3	2
11011.0466	7.56E-26	2.72E-04	0.094	0.43	0.72	0	0	0	5	2	3	0	0	3	6	0	6
11011.332	1.97E-25	4.66E-04	0.094	0.47	0.74	0	0	0	3	3	0	0	0	3	4	1	3
11011.4071	6.69E-24	3.40E-02	0.1	0.51	0.75	0	0	0	2	1	1	0	0	3	2	1	2
11017.1068	2.08E-23	1.29E-01	0.095	0.46	0.71	0	0	0	2	2	0	0	0	3	2	2	1
11018.1077	5.57E-26	1.16E-04	0.103	0.6	0.74	0	0	0	3	0	3	0	0	3	2	2	0
11018.528	2.39E-24	1.16E-02	0.086	0.44	0.7	0	0	0	3	2	2	1	0	2	4	3	1
11019.5353	3.40E-25	1.93E-02	0.087	0.46	0.73	0	0	0	7	3	5	0	0	3	7	3	4
11019.9662	6.15E-23	1.27E-01	0.093	0.46	0.7	0	0	0	2	2	1	0	0	3	2	2	0
11020.3741	1.91E-25	4.51E-04	0.093	0.46	0.75	0	0	0	5	0	5	1	0	2	5	3	2

11022.5766	4.07E-26	1.96E-03	0.042	0.33	0.05	0	0	0	9	1	8	1	0	2	10	2	9
11022.9353	6.40E-25	4.33E-03	0.092	0.45	0.8	0	0	0	4	2	2	1	0	2	5	3	3
11023.4023	9.03E-24	5.64E-02	0.094	0.47	0.71	0	0	0	3	2	2	0	0	3	3	2	1
11023.4023	4.60E-23	1.01E-01	0.104	0.47	0.7	0	0	0	1	1	0	0	0	3	1	1	1
11024.6943	4.59E-26	1.95E-03	0.087	0.34	0.68	0	0	0	6	4	2	0	0	3	7	2	5
11025.2192	7.76E-25	2.76E-03	0.098	0.47	0.81	0	0	0	3	1	3	1	0	2	4	2	2
11027.3132	2.84E-25	1.26E-03	0.086	0.53	0.75	0	0	0	2	2	0	0	0	3	3	0	3
11027.8448	8.77E-25	5.94E-03	0.093	0.48	0.72	0	0	0	4	2	2	0	0	3	5	0	5
11029.265	7.80E-26	1.47E-03	0.087	0.49	0.73	0	0	0	7	3	4	0	0	3	8	1	7
11029.5754	8.75E-24	2.08E-02	0.073	0.47	0.61	0	0	0	3	3	0	1	0	2	4	4	1
11029.7704	2.87E-24	2.05E-02	0.073	0.39	0.58	0	0	0	3	3	1	1	0	2	4	4	0
11030.9522	1.20E-25	1.13E-03	0.095	0.38	0.72	0	0	0	4	3	1	0	0	3	5	1	4
11031.1961	1.16E-23	2.96E-02	0.095	0.51	0.72	0	0	0	4	2	3	0	0	3	4	2	2
11031.8186	2.29E-26	3.96E-04	0.085	0.5	0.71	0	0	0	6	1	5	1	0	2	6	4	2
11032.1834	1.66E-24	5.98E-03	0.091	0.43	0.8	0	0	0	5	2	3	1	0	2	6	3	4
11032.3154	1.31E-24	2.19E-03	0.094	0.52	0.74	0	0	0	3	2	1	0	0	3	4	0	4
11032.5575	3.17E-25	1.33E-02	0.088	0.45	0.69	0	0	0	8	3	6	0	0	3	8	3	5
11032.9137	7.64E-26	2.59E-04	0.091	0.43	0.76	0	0	0	5	1	4	1	0	2	5	4	1
11033.9746	1.54E-23	9.88E-02	0.103	0.53	0.71	0	0	0	1	1	1	0	0	3	1	1	0

11036.6414	3.78E-25	7.59E-03	0.092	0.45	0.73	0	0	0	6	2	4	1	0	2	7	3	5
11038.0066	4.46E-25	6.30E-03	0.084	0.43	0.63	0	0	0	7	2	5	1	0	2	8	3	6
11038.4691	8.45E-26	9.26E-04	0.072	0.39	0.7	0	0	0	7	1	6	1	0	2	7	4	3
11039.3908	6.30E-26	5.54E-03	0.068	0.55	0.43	0	0	0	9	2	7	1	0	2	10	3	8
11041.0061	5.29E-26	1.41E-03	0.089	0.35	0.72	0	0	0	6	3	3	0	0	3	7	1	6
11041.2205	9.42E-26	2.75E-03	0.084	0.48	0.64	0	0	0	7	4	3	0	0	3	8	2	6
11041.4959	3.20E-25	1.57E-03	0.091	0.44	0.72	0	0	0	5	3	2	0	0	3	6	1	5
11043.0033	1.62E-24	1.79E-02	0.091	0.48	0.73	0	0	0	5	2	4	0	0	3	5	2	3
11043.0703	2.01E-23	3.17E-02	0.104	0.46	0.74	0	0	0	2	1	2	0	0	3	2	1	1
11045.3605	3.22E-24	6.76E-03	0.089	0.51	0.73	0	0	0	4	2	3	1	0	2	5	3	2
11046.7701	2.65E-26	9.74E-03	0.08	0.43	0.49	0	0	0	9	3	7	0	0	3	9	3	6
11048.4789	1.59E-24	1.51E-02	0.083	0.47	0.68	0	0	0	4	3	1	1	0	2	5	4	2
11049.8578	4.30E-24	1.35E-02	0.076	0.43	0.56	0	0	0	4	3	2	1	0	2	5	4	1
11055.4711	1.24E-23	6.67E-02	0.104	0.44	0.76	0	0	0	0	0	0	0	0	3	1	0	1
11056.1481	3.47E-24	1.60E-02	0.101	0.54	0.74	0	0	0	3	1	3	0	0	3	3	1	2
11057.5401	1.89E-24	1.15E-02	0.09	0.46	0.69	0	0	0	6	2	5	0	0	3	6	2	4
11058.8092	3.06E-24	4.82E-02	0.057	0.5	0.42	0	0	0	4	4	0	1	0	2	5	5	1
11058.823	1.78E-24	9.35E-03	0.065	0.44	0.41	0	0	0	4	4	1	1	0	2	5	5	0
11059.6273	1.40E-26	3.24E-05	0.102	0.46	0.77	0	0	0	2	0	2	1	0	2	3	3	1

11060.1491	2.18E-26	7.74E-03	0.073	0.36	0.45	0	0	0	10	3	8	0	0	3	10	3	7
11065.1457	2.33E-24	1.15E-02	0.085	0.42	0.72	0	0	0	5	3	2	1	0	2	6	4	3
11068.4575	5.32E-25	7.77E-04	0.1	0.5	0.8	0	0	0	4	1	4	1	0	2	5	2	3
11069.4457	1.57E-23	6.07E-02	0.099	0.47	0.75	0	0	0	1	1	1	0	0	3	2	1	2
11069.7511	2.64E-26	4.25E-04	0.083	0.38	0.7	0	0	0	7	2	5	1	0	2	7	5	2
11070.7528	6.26E-25	9.02E-03	0.079	0.36	0.52	0	0	0	5	3	3	1	0	2	6	4	2
11071.5226	4.92E-26	1.37E-02	0.054	0.32	0.18	0	0	0	7	7	0	0	0	3	8	7	1
11071.9071	5.46E-24	9.76E-03	0.097	0.58	0.7	0	0	0	4	1	4	0	0	3	4	1	3
11072.865	2.53E-25	8.57E-03	0.084	0.43	0.63	0	0	0	7	2	6	0	0	3	7	2	5
11076.1783	6.35E-23	7.70E-02	0.101	0.47	0.71	0	0	0	1	0	1	0	0	3	2	0	2
11076.9355	1.43E-24	1.15E-02	0.067	0.32	0.41	0	0	0	5	4	1	1	0	2	6	5	2
11077.0865	4.61E-25	1.11E-02	0.068	0.31	0.38	0	0	0	5	4	2	1	0	2	6	5	1
11077.6421	3.03E-25	2.86E-03	0.088	0.44	0.76	0	0	0	5	2	4	1	0	2	6	3	3
11077.8259	3.18E-25	8.55E-03	0.084	0.41	0.76	0	0	0	6	3	3	1	0	2	7	4	4
11080.1954	4.42E-23	5.87E-02	0.101	0.47	0.67	0	0	0	1	1	0	0	0	3	2	1	1
11080.2306	4.60E-25	2.11E-02	0.043	0.43	0.25	0	0	0	5	5	1	1	0	2	6	6	0
11080.2428	2.84E-25	4.34E-03	0.051	0.43	0.25	0	0	0	5	5	0	1	0	2	6	6	1
11082.0851	1.23E-25	2.13E-02	0.044	0.34	0.27	0	0	0	6	6	0	0	0	3	7	6	1
11082.1963	4.10E-26	2.55E-04	0.092	0.57	0.77	0	0	0	7	0	7	1	0	2	7	3	4

11083.1804	4.78E-25	2.18E-03	0.104	0.44	0.72	0	0	0	2	0	2	0	0	3	2	2	1
11085.7768	2.99E-24	4.49E-03	0.101	0.61	0.73	0	0	0	3	0	3	0	3	0	3	2	2
11086.8568	2.86E-25	6.74E-03	0.094	0.36	0.57	0	0	0	8	2	7	0	0	3	8	2	6
11087.3665	6.75E-23	7.67E-02	0.096	0.46	0.74	0	0	0	2	1	2	0	0	3	3	1	3
11087.6369	3.21E-23	4.77E-02	0.094	0.46	0.68	0	0	0	2	2	1	0	0	3	3	2	2
11088.1688	9.62E-25	6.94E-03	0.091	0.46	0.63	0	0	0	5	1	5	0	0	3	5	1	4
11089.6372	9.04E-26	5.87E-02	0.039	0.33	0.11	0	0	0	8	7	2	0	0	3	9	7	3
11091.4097	1.06E-24	5.63E-03	0.09	0.46	0.65	0	0	0	4	0	4	0	0	3	4	2	3
11093.3849	2.48E-23	8.09E-02	0.097	0.46	0.73	0	0	0	2	0	2	0	0	3	3	0	3
11093.5398	1.06E-23	4.76E-02	0.098	0.48	0.74	0	0	0	2	2	0	0	0	3	3	2	1
11093.699	5.75E-25	4.86E-03	0.068	0.44	0.56	0	0	0	6	3	4	1	0	2	7	4	3
11094.5376	1.36E-25	5.84E-03	0.072	0.32	0.44	0	0	0	6	4	2	1	0	2	7	5	3
11095.4386	2.99E-25	4.27E-03	0.077	0.32	0.34	0	0	0	6	4	3	1	0	2	7	5	2
11096.9124	5.62E-24	4.06E-02	0.082	0.45	0.63	0	0	0	3	3	1	0	0	3	4	3	2
11098.151	2.60E-26	5.00E-03	0.069	0.3	0.49	0	0	0	9	2	7	0	0	3	9	4	6
11098.269	9.43E-26	1.11E-02	0.073	0.38	0.19	0	0	0	7	6	1	0	0	3	8	6	2
11098.308	3.26E-25	5.70E-03	0.083	0.59	0.61	0	0	0	6	1	5	0	0	3	6	3	4
11098.3494	9.94E-25	8.09E-02	0.055	0.42	0.21	0	0	0	6	5	1	1	0	2	7	6	2
11098.4093	3.05E-24	1.40E-01	0.054	0.28	0.41	0	0	0	5	5	1	0	0	3	6	5	2

111098.7655	1.64E-23	3.95E-02	0.08	0.47	0.7	0	0	0	3	3	0	0	0	3	4	3	1
111099.1506	4.56E-25	5.05E-03	0.074	0.5	0.47	0	0	0	7	1	6	0	0	3	7	3	5
111099.2937	7.16E-24	3.78E-02	0.073	0.41	0.55	0	0	0	4	4	1	0	0	3	5	4	2
111099.6503	2.36E-24	5.65E-03	0.086	0.53	0.52	0	0	0	5	0	5	0	0	3	5	2	4
111099.7007	2.34E-24	3.71E-02	0.07	0.25	0.57	0	0	0	4	4	0	0	0	3	5	4	1
111100.9898	7.99E-25	2.75E-03	0.092	0.47	0.68	0	0	0	5	1	4	0	0	3	5	3	3
111103.0105	9.97E-26	6.97E-03	0.067	0.33	0.3	0	0	0	8	1	7	0	0	3	8	3	6
111103.0576	1.57E-24	5.76E-03	0.084	0.5	0.53	0	0	0	6	1	6	0	0	3	6	1	5
111103.2506	1.99E-23	7.36E-02	0.098	0.46	0.72	0	0	0	2	1	1	0	0	3	3	1	2
111103.617	2.31E-23	8.34E-02	0.092	0.47	0.63	0	0	0	3	1	3	0	0	3	4	1	4
111105.3682	2.00E-26	2.47E-03	0.077	0.33	0.53	0	0	0	8	2	6	0	0	3	8	4	5
111106.6342	1.85E-25	1.27E-03	0.092	0.59	0.72	0	0	0	4	1	3	0	0	3	4	3	2
111106.9313	1.70E-25	5.02E-03	0.078	0.32	0.52	0	0	0	7	4	3	1	0	2	8	5	4
111107.1606	1.35E-23	6.67E-02	0.091	0.47	0.62	0	0	0	3	2	2	0	0	3	4	2	3
111107.7097	7.26E-23	8.50E-02	0.094	0.47	0.71	0	0	0	3	0	3	0	0	3	4	0	4
111109.3879	9.15E-26	4.96E-03	0.054	0.58	0.16	0	0	0	9	1	8	0	0	3	9	3	7
111109.4475	4.68E-25	5.14E-03	0.077	0.29	0.4	0	0	0	6	0	6	0	0	3	6	2	5
111111.7143	2.99E-26	8.17E-03	0.055	0.61	0.13	0	0	0	8	6	3	0	0	3	9	6	4
111113.7536	3.03E-25	5.47E-04	0.09	0.49	0.74	0	0	0	3	1	2	0	0	3	3	3	1

11115.5347	1.06E-25	5.63E-04	0.089	0.25	0.76	0	0	0	6	2	5	1	0	2	7	3	4
11115.939	1.14E-25	1.85E-03	0.083	0.44	0.58	0	0	0	7	2	5	0	0	3	7	4	4
11116.0795	2.45E-25	4.61E-03	0.073	0.34	0.4	0	0	0	7	1	7	0	0	3	7	1	6
11116.3269	7.03E-26	4.32E-04	0.096	0.76	0.74	0	0	0	5	1	5	1	0	2	6	2	4
11116.6624	3.24E-24	1.42E-02	0.09	0.5	0.73	0	0	0	4	0	4	1	0	2	5	3	3
11117.9304	1.90E-23	6.03E-02	0.082	0.44	0.56	0	0	0	4	3	2	0	0	3	5	3	3
11118.3225	5.85E-23	8.63E-02	0.085	0.44	0.49	0	0	0	4	1	4	0	0	3	5	1	5
11119.4022	3.84E-23	6.50E-02	0.093	0.47	0.77	0	0	0	3	2	1	0	0	3	4	2	2
11119.982	6.90E-25	4.32E-03	0.066	0.38	0.3	0	0	0	7	0	7	0	0	3	7	2	6
11120.9795	2.36E-24	6.42E-02	0.06	0.38	0.3	0	0	0	6	5	2	0	0	3	7	5	3
11121.0368	2.39E-24	5.81E-02	0.073	0.24	0.44	0	0	0	5	4	2	0	0	3	6	4	3
11121.1464	4.06E-26	1.45E-03	0.095	0.33	0.78	0	0	0	8	0	8	1	0	2	8	3	5
11121.2671	7.60E-25	6.21E-02	0.059	0.31	0.33	0	0	0	6	5	1	0	0	3	7	5	2
11121.5717	1.69E-23	7.37E-02	0.087	0.53	0.57	0	0	0	4	0	4	0	0	3	5	0	5
11122.72	7.06E-24	5.74E-02	0.078	0.45	0.54	0	0	0	5	4	1	0	0	3	6	4	2
11123.3793	5.60E-23	7.87E-02	0.096	0.47	0.75	0	0	0	3	1	2	0	0	3	4	1	3
11123.7324	6.09E-24	5.84E-02	0.088	0.48	0.74	0	0	0	4	3	1	0	0	3	5	3	2
11124.6353	3.54E-23	7.55E-02	0.086	0.44	0.52	0	0	0	4	2	3	0	0	3	5	2	4
11126.7061	1.05E-26	6.03E-05	0.085	0.42	0.64	0	0	0	6	1	6	1	0	2	6	4	3

11127.4587	3.28E-25	3.91E-03	0.06	0.34	0.26	0	0	0	8	1	8	0	0	3	8	1	7
11128.3783	3.13E-26	7.67E-04	0.086	0.42	0.64	0	0	0	6	2	4	0	0	3	6	4	3
11131.0729	1.73E-24	2.12E-03	0.107	0.46	0.73	0	0	0	1	0	1	0	0	3	2	2	0
11131.9896	1.49E-23	9.14E-02	0.075	0.48	0.33	0	0	0	5	1	5	0	0	3	6	1	6
11132.2091	4.23E-23	8.62E-02	0.076	0.43	0.38	0	0	0	5	0	5	0	0	3	6	0	6
11133.481	6.37E-26	2.28E-03	0.061	0.33	0.2	0	0	0	8	0	8	0	0	3	8	2	7
11137.2435	4.88E-24	7.11E-02	0.082	0.47	0.48	0	0	0	5	3	3	0	0	3	6	3	4
11137.3082	1.51E-25	3.80E-03	0.056	0.3	0.12	0	0	0	9	0	9	0	0	3	9	2	8
11137.4985	4.11E-26	3.10E-03	0.053	0.3	0.14	0	0	0	9	1	9	0	0	3	9	1	8
11139.2973	1.38E-23	7.81E-02	0.091	0.44	0.73	0	0	0	4	1	3	0	0	3	5	1	4
11139.935	8.57E-24	8.16E-02	0.081	0.48	0.42	0	0	0	5	2	4	0	0	3	6	2	5
11140.8889	9.04E-26	3.93E-04	0.088	0.5	0.78	0	0	0	5	2	3	0	0	3	5	4	2
11141.6259	4.79E-24	6.90E-02	0.074	0.42	0.39	0	0	0	6	4	3	0	0	3	7	4	4
11141.6259	2.94E-25	4.15E-04	0.093	0.47	0.81	0	0	0	3	1	2	1	0	2	4	4	1
11142.1437	4.34E-25	7.21E-02	0.062	0.33	0.25	0	0	0	7	5	3	0	0	3	8	5	4
11143.164	1.57E-24	8.69E-02	0.055	0.38	0.32	0	0	0	7	5	2	0	0	3	8	5	3
11143.2036	2.73E-23	8.72E-02	0.066	0.42	0.18	0	0	0	6	1	6	0	0	3	7	1	7
11143.4319	1.07E-23	7.40E-02	0.092	0.49	0.8	0	0	0	4	2	2	0	0	3	5	2	3
11143.8955	9.44E-24	9.04E-02	0.066	0.42	0.19	0	0	0	6	0	6	0	0	3	7	0	7

11145.1594	2.26E-26	1.08E-04	0.098	0.77	0.77	0	0	0	3	1	3	0	0	3	3	0
11146.4207	1.43E-24	8.41E-02	0.042	0.4	0.06	0	0	0	10	1	10	0	0	3	10	9
11146.4207	6.25E-26	2.72E-03	0.082	0.42	0.6	0	0	0	6	4	2	0	0	3	7	4
11149.6823	1.36E-23	6.76E-02	0.087	0.49	0.77	0	0	0	5	3	2	0	0	3	6	3
11150.8524	2.60E-23	7.63E-02	0.086	0.43	0.63	0	0	0	5	1	4	0	0	3	6	1
11151.7826	1.16E-26	1.93E-04	0.089	0.44	0.73	0	0	0	4	2	2	0	0	3	4	1
11153.3138	1.63E-23	8.74E-02	0.074	0.42	0.31	0	0	0	6	2	5	0	0	3	7	2
11153.3472	1.31E-24	2.69E-03	0.087	0.43	0.63	0	0	0	5	0	5	1	0	2	6	3
11154.2751	1.29E-25	1.95E-02	0.03	0.26	0.03	0	0	0	11	0	11	0	0	3	11	2
11154.3851	9.17E-24	7.84E-02	0.081	0.44	0.41	0	0	0	6	3	4	0	0	3	7	3
11154.5222	5.58E-24	9.32E-02	0.053	0.43	0.04	0	0	0	7	1	7	0	0	3	8	1
11154.7645	1.68E-23	9.32E-02	0.056	0.41	0.04	0	0	0	7	0	7	0	0	3	8	0
11155.6019	5.92E-25	1.80E-02	0.081	0.4	0.74	0	0	0	7	2	6	1	0	2	8	3
11156.8248	4.05E-25	2.30E-03	0.095	0.46	0.78	0	0	0	4	1	3	1	0	2	5	4
11159.3451	6.74E-26	1.22E-04	0.094	0.44	0.69	0	0	0	4	1	4	0	0	3	4	3
11159.6131	1.24E-24	4.08E-03	0.117	0.46	0.73	0	0	0	2	0	2	0	0	3	3	2
11159.6536	5.09E-24	7.81E-02	0.078	0.5	0.5	0	0	0	6	1	5	0	0	3	7	1
11160.5355	8.41E-25	7.38E-02	0.07	0.35	0.33	0	0	0	7	4	4	0	0	3	8	4
11161.7784	5.80E-25	7.47E-02	0.062	0.31	0.23	0	0	0	8	5	4	0	0	3	9	5

11163.9407	2.11E-23	7.80E-02	0.094	0.43	0.81	0	0	0	5	2	3	0	0	3	6	2	4
11164.6399	1.99E-25	7.73E-02	0.063	0.33	0.38	0	0	0	8	5	3	0	0	3	9	5	4
11164.7335	8.93E-24	9.59E-02	0.047	0.34	-0.07	0	0	0	8	1	8	0	0	3	9	1	9
11164.8443	2.91E-24	9.37E-02	0.046	0.33	-0.08	0	0	0	8	0	8	0	0	3	9	0	9
11167.4072	8.24E-24	8.15E-02	0.068	0.38	0.31	0	0	0	7	1	6	0	0	3	8	1	7
11167.9332	2.32E-24	7.08E-02	0.062	0.38	0.18	0	0	0	7	2	6	0	0	3	8	2	7
11167.9735	1.58E-24	5.07E-03	0.097	0.42	0.66	0	0	0	6	1	6	1	0	2	7	2	5
11169.2001	1.59E-24	8.18E-02	0.072	0.36	0.32	0	0	0	7	3	5	0	0	3	8	3	6
11171.4936	2.42E-24	7.23E-02	0.083	0.43	0.65	0	0	0	7	4	3	0	0	3	8	4	4
11171.8753	3.72E-24	7.96E-02	0.056	0.37	0.05	0	0	0	8	2	7	0	0	3	9	2	8
11172.7118	1.17E-26	5.35E-05	0.096	0.47	0.73	0	0	0	3	1	3	1	0	2	4	4	0
11174.0093	1.44E-24	9.86E-02	0.036	0.35	-0.18	0	0	0	9	1	9	0	0	3	10	1	10
11174.048	4.26E-24	9.76E-02	0.037	0.26	-0.18	0	0	0	9	0	9	0	0	3	10	0	10
11174.5007	1.33E-24	3.91E-03	0.097	0.45	0.74	0	0	0	5	1	4	1	0	2	6	4	3
11174.6805	2.71E-24	7.42E-02	0.086	0.41	0.76	0	0	0	6	3	3	0	0	3	7	3	4
11174.8194	1.34E-24	8.49E-02	0.056	0.35	0.09	0	0	0	8	1	7	0	0	3	9	1	8
11177.364	1.13E-24	7.66E-02	0.067	0.32	0.25	0	0	0	8	4	5	0	0	3	9	4	6
11179.5917	7.08E-26	7.22E-02	0.054	0.3	0.15	0	0	0	9	5	5	0	0	3	10	5	6
11179.6986	3.84E-24	7.90E-02	0.089	0.52	0.76	0	0	0	6	2	4	0	0	3	7	2	5

11180.1505	2.12E-26	1.78E-04	0.079	0.41	0.64	0	0	0	6	2	5	0	0	3	6	4	2
11180.2644	1.01E-25	2.93E-02	0.056	0.3	0.13	0	0	0	9	3	7	0	0	3	10	3	8
11181.8972	1.79E-24	8.86E-02	0.045	0.32	-0.09	0	0	0	9	1	8	0	0	3	10	1	9
11182.353	2.27E-24	8.76E-02	0.063	0.33	0.23	0	0	0	8	3	6	0	0	3	9	3	7
11182.3926	2.23E-24	1.20E-01	0.033	0.28	-0.24	0	0	0	10	1	10	0	0	3	11	1	11
11185.4289	1.34E-25	4.62E-02	0.07	0.3	0.43	0	0	0	9	5	4	0	0	3	10	5	5
11187.7708	7.15E-25	9.20E-02	0.037	0.23	-0.14	0	0	0	10	2	9	0	0	3	11	2	10
11188.3307	2.33E-25	8.97E-02	0.04	0.24	-0.21	0	0	0	10	1	9	0	0	3	11	1	10
11189.9029	7.26E-25	1.01E-01	0.023	0.26	-0.29	0	0	0	11	0	11	0	0	3	12	0	12
11189.9029	2.42E-25	1.01E-01	0.027	0.26	-0.29	0	0	0	11	1	11	0	0	3	12	1	12
11190.0468	5.40E-24	7.84E-02	0.085	0.48	0.63	0	0	0	7	2	5	0	0	3	8	2	6
11192.0683	1.72E-25	9.14E-02	0.06	0.31	0.18	0	0	0	9	4	6	0	0	3	10	4	7
11192.263	2.54E-25	9.53E-04	0.084	0.46	0.7	0	0	0	2	1	1	0	0	3	3	3	0
11192.7179	2.41E-25	2.33E-03	0.079	0.41	0.53	0	0	0	6	0	6	1	0	2	7	3	5
11193.1097	2.51E-25	6.80E-02	0.048	0.28	0.04	0	0	0	10	3	8	0	0	3	11	3	9
11193.9254	9.35E-26	1.03E-01	0.029	0.26	-0.24	0	0	0	11	2	10	0	0	3	12	2	11
11194.2042	2.59E-25	9.45E-02	0.03	0.23	-0.29	0	0	0	11	1	10	0	0	3	12	1	11
11194.5932	2.23E-26	7.74E-04	0.077	0.38	0.59	0	0	0	7	2	6	0	0	3	7	4	3
11194.7969	3.39E-24	4.04E-03	0.099	0.55	0.77	0	0	0	3	0	3	0	0	3	4	2	2

11195.2569	7.03E-26	7.16E-02	0.059	0.24	0.11	0	0	0	10	5	6	0	0	3	11	5	7
11195.7978	7.55E-25	7.81E-02	0.075	0.39	0.47	0	0	0	8	2	6	0	0	3	9	2	7
11196.317	3.99E-24	7.77E-02	0.091	0.49	0.73	0	0	0	7	3	4	0	0	3	8	3	5
11196.3723	3.48E-25	7.43E-02	0.082	0.33	0.65	0	0	0	8	4	4	0	0	3	9	4	5
11196.7399	3.64E-25	1.45E-01	0.027	0.24	-0.34	0	0	0	12	1	12	0	0	3	13	1	13
11199.0504	8.60E-25	7.78E-02	0.064	0.35	0.32	0	0	0	9	2	7	0	0	3	10	2	8
11199.2203	1.20E-25	1.37E-01	0.025	0.66	-0.33	0	0	0	12	2	11	0	0	3	13	2	12
11199.5416	5.11E-26	1.28E-01	0.039	0.26	-0.05	0	0	0	11	3	9	0	0	3	12	3	10
11201.7485	1.30E-25	1.02E-01	0.055	0.26	0.13	0	0	0	10	2	8	0	0	3	11	2	9
11203.6326	3.54E-26	1.38E-01	0.022	0.21	-0.51	0	0	0	13	1	12	0	0	3	14	1	13
11203.8374	9.51E-26	7.78E-02	0.045	0.36	-0.08	0	0	0	11	2	9	0	0	3	12	2	10
11204.164	4.09E-26	1.16E-01	0.042	0.24	-0.16	0	0	0	12	3	10	0	0	3	13	3	11
11205.6696	1.80E-25	9.39E-02	0.052	0.42	0.09	0	0	0	10	4	7	0	0	3	11	4	8
11207.5385	6.14E-26	9.20E-05	0.093	0.44	0.72	0	0	0	4	1	4	1	0	2	5	4	1
11207.6234	4.15E-25	4.82E-04	0.097	0.39	0.74	0	0	0	2	1	2	0	0	3	3	3	1
11208.2418	4.67E-25	1.01E-02	0.082	0.43	0.65	0	0	0	8	2	7	1	0	2	9	3	6
11210.8188	1.81E-24	2.59E-03	0.095	0.49	0.76	0	0	0	3	1	2	0	0	3	4	3	1
11212.8447	5.59E-25	8.04E-02	0.088	0.43	0.69	0	0	0	8	3	5	0	0	3	9	3	6
11218.6864	1.22E-25	2.05E-03	0.082	0.34	0.61	0	0	0	7	1	7	1	0	2	8	2	6

11219.0401	4.19E-25	8.22E-02	0.089	0.44	0.61	0	0	0	9	4	5	0	0	3	10	4	6
11223.3575	5.84E-25	7.87E-02	0.085	0.39	0.63	0	0	0	9	3	6	0	0	3	10	3	7
11223.7402	3.82E-25	3.82E-03	0.078	0.39	0.57	0	0	0	7	1	6	1	0	2	8	4	5

Appendix B

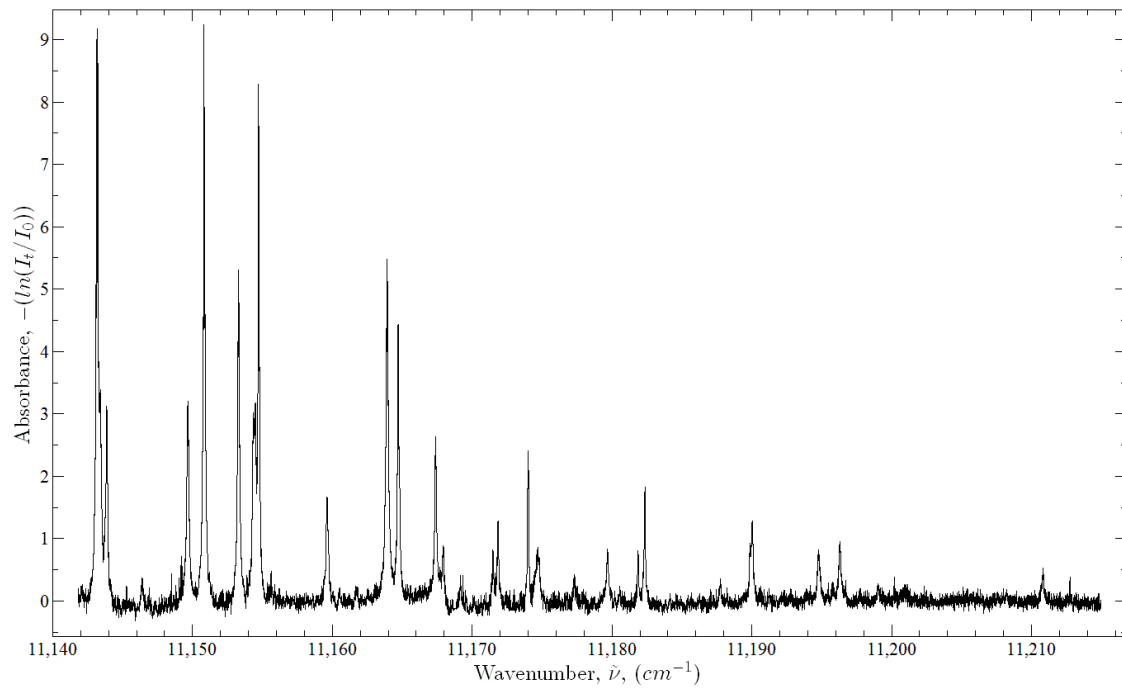


Figure 13: Atmospheric absorption spectrum in the region surrounding the Cs DPAL emission line, taken from 1545 to 1700 on 17 October 2012. The scan ranges from 11,140 to 11,210 cm^{-1} and contains ~ 30 absorption line, a number of which are obscured by baseline noise.

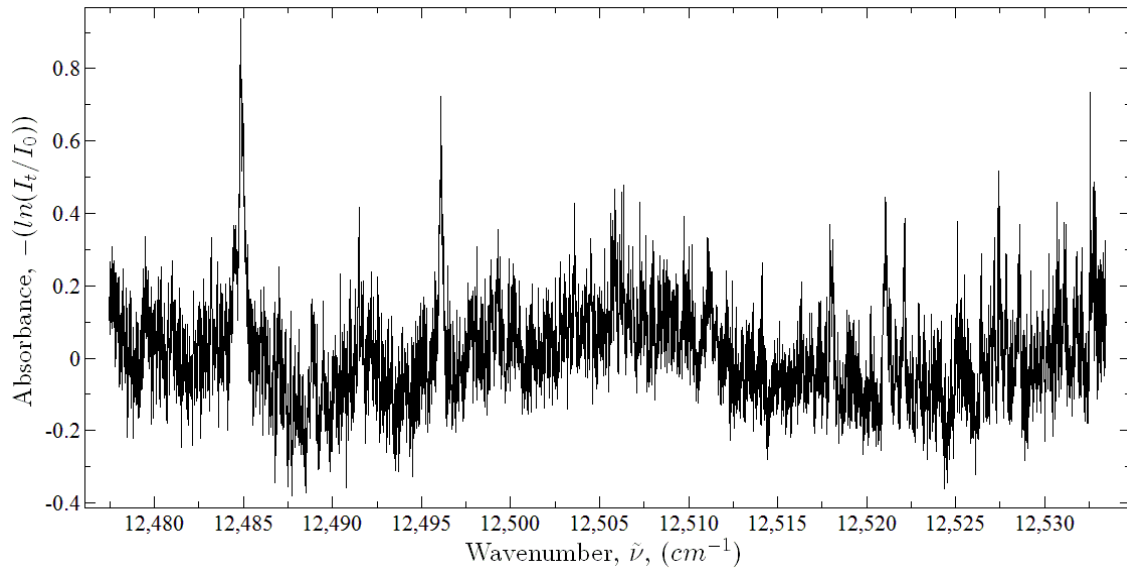


Figure 14: Atmospheric absorption spectra from 12,480 to 12,530 cm^{-1} collected from 1628 to 1909 on 19 October 2012. This spectrum contains ~ 25 weak H_2O absorption lines, many of which are obscured by the noise in the baseline.

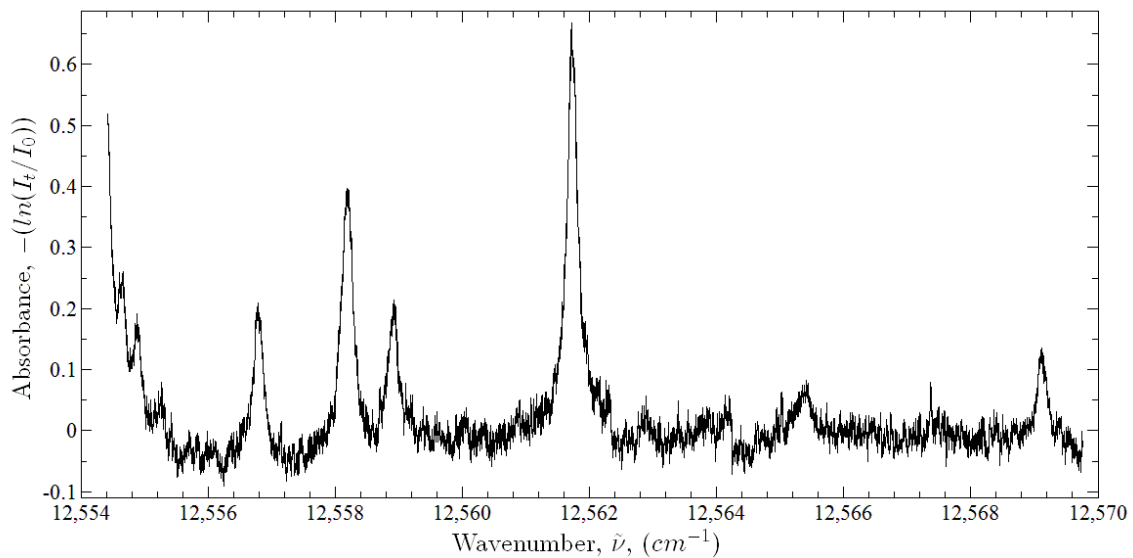


Figure 15: Atmospheric absorption spectra from 12,554 to 12,570 cm^{-1} collected from 2159 on 19 October 2012 to 0050 on 20 October 2012. The lower noise level is due to the signal averaging used. With 6 scans per piezo range, the signal to noise ratio was improved significantly.

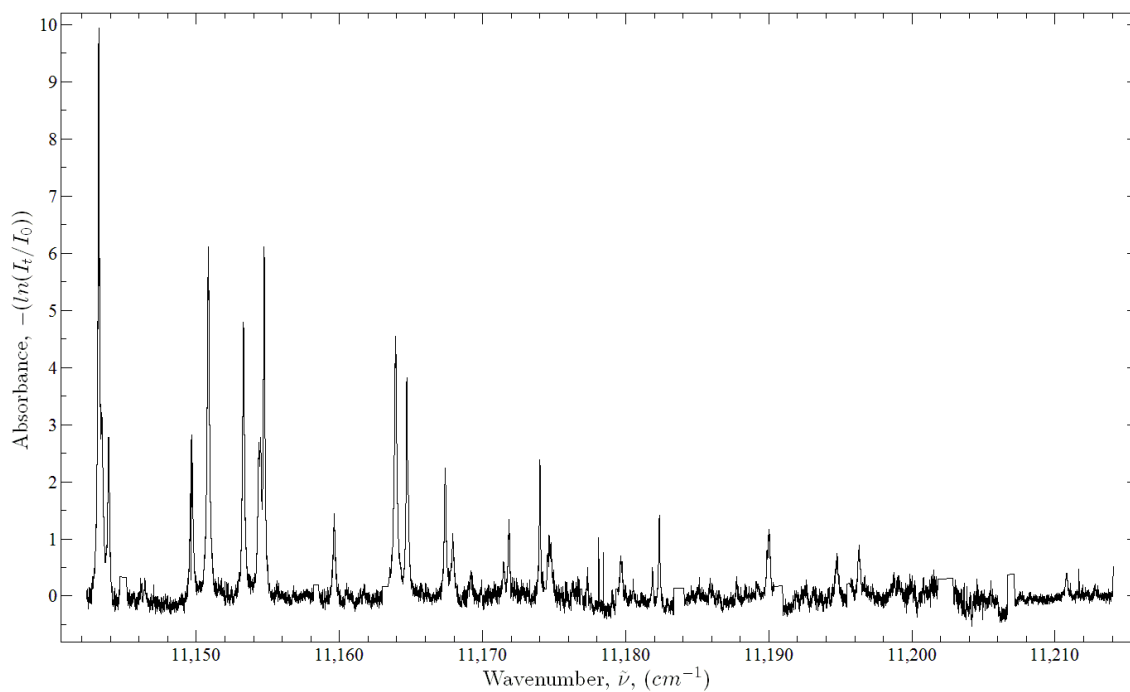


Figure 16: Atmospheric absorption spectra in the Cs DPAL emission region, from 11,150 to 11,210 cm^{-1} , collected from 1905 to 2136 on 22 October 2012. This spectrum contains ~ 30 strong H_2O absorption lines, some of which are obscured by the noise in the baseline, as well as the Cs doublet located at $\sim 11,182 \text{ cm}^{-1}$.

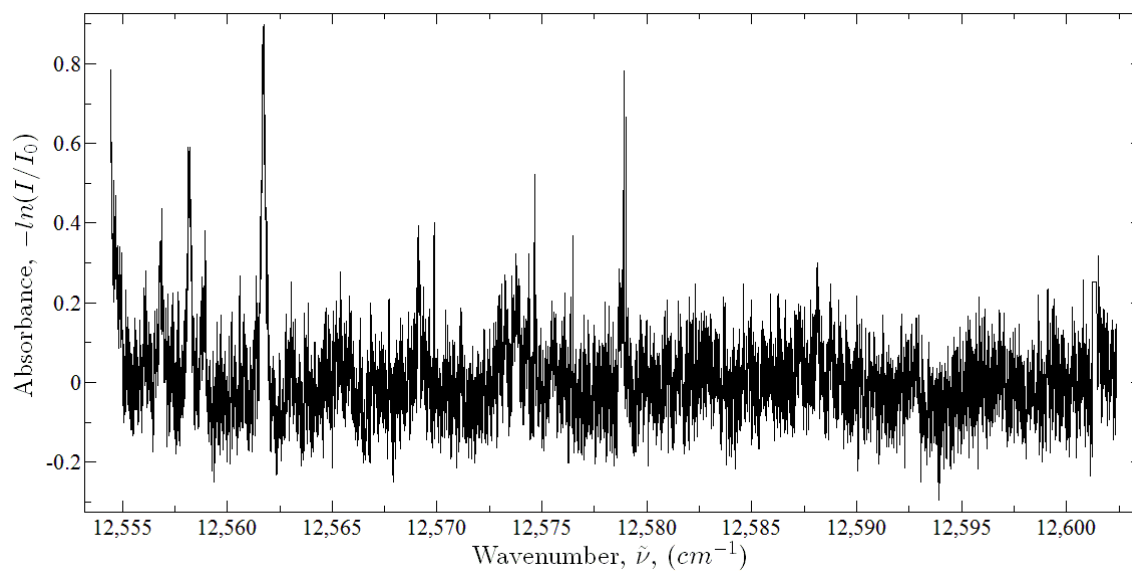


Figure 17: Sample of data collected in the Rb region, from 12,555 to 12,600 cm^{-1} , on 23 October 2012 from 1515 to 1542 consisting of ~25 weak H_2O absorption lines as well as the Rb D_1 emission lines at ~12,578 cm^{-1} .

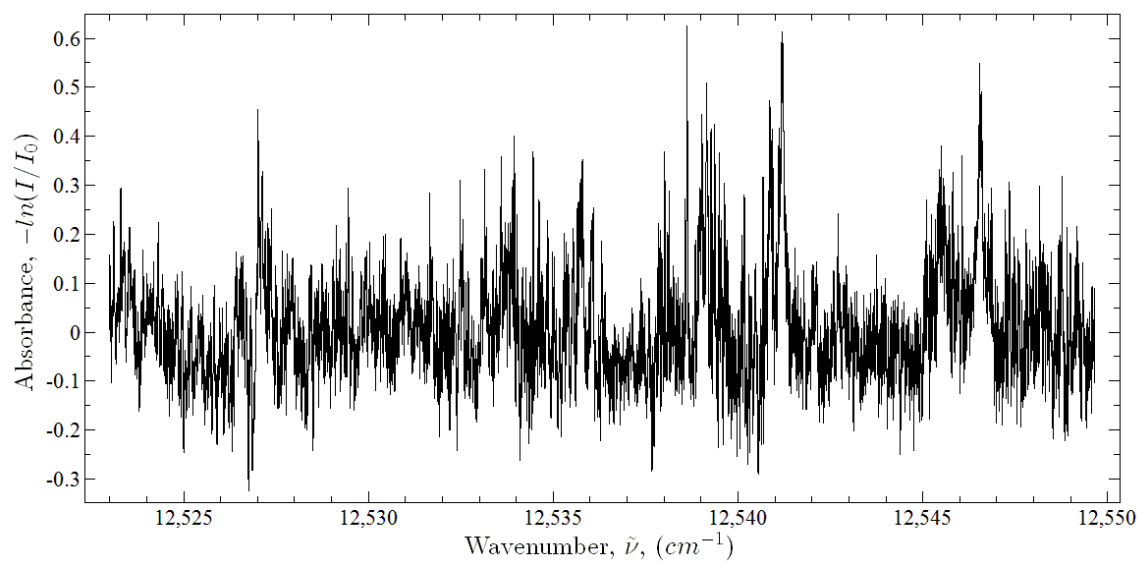


Figure 18: Atmospheric absorption spectra from 12,525 to 12,550 cm^{-1} collected from 1551 to 1705 on 23 October 2012. This spectrum contains over 30 weak H_2O absorption lines, many of which are obscured by the noise in the baseline.

Bibliography

1. W. F. Krupke, R. J. Beach, V. K. Kanz, and S. A. Payne, "Diode Pumpable Rubidium Laser," in *Advanced Solid-State Photonics*, J. Zayhowski, ed., Vol. 83 of *OSA Trends in Optics and Photonics* (Optical Society of America, 2003), paper 121.
2. Ralph H. Page, Raymond J. Beach, V. Keith Kanz, and William F. Krupke, "Multimode-diode-pumped gas (alkali-vapor) laser," *Opt. Lett.* 31, 353-355 (2006)
3. R. J. Beach, W. F. Krupke, V. K. Kanz, M. A. Dubinskii, and L. D. Merkle, "End-pumped 895 nm Cs laser", *Advanced Solid State Photonics (ASSP) meeting*, Feb 2-4, 2004.
4. Zhdanov, B., C. Maes, T. Ehrenreich, A. Havko, N. Koval, T. Meeker, B. Worker, B. Flusche, and RJ Knize. "Optically pumped potassium laser". *Optics Communications*, 270(2):353-355, 2007.
5. Bogachev, A.V., S. G. Garanin, A.M. Dudov, V.A. Eroshenko, S.M. Kulikov, G.T. Mikaelian, V.A. Panarin, V.O. Pautov, A.V. Rus, and S.A. Sukharev. "Diode-pumped caesium vapour laser with closed-cycle laser-active medium circulation". *Quantum Electronics*, 42(2):95-98, 2012.
6. Bernath, P. F. *Spectra of atoms and molecules*. Oxford University Press, USA, 2005.
7. Verdeyen, J. T. *Laser Electronics*. Prentice Hall, USA, 1995.
8. L. S. Rothman, C. P. Rinsland, A. Goldman, S. T. Massie, D. P. Edwards, J.-M. Flaud, A. Perrin, C. Camy-Peyret, V. Dana, J.-Y. Mandin, J. Schroeder, A. Mccann, R. R. Gamache, R. B. Wattson, K. Yoshino, K. V. Chance, K. W. Jucks, L. R. Brown, V. Nemtchinov and P. Varanasi. "The Hitran Molecular Spectroscopic Database and Hawks (HITRAN Atmospheric Workstation):1996 Edition". *Journal of Quantitative Spectroscopy and Radiative Transfer*, 60(5):665-710, 1998.
9. Goff, J. A., and S. Gratch. "Low-pressure properties of water from 160 to 212 °F". *Transactions of the American Society of Heating and Ventilating Engineers*, 95-122, 1946.
10. G. P. Perram, S. J. Cusumano, R. L. Hengehold, and S. T. Fiorino. *An Introduction to Laser Weapon Systems*. Directed Energy Professional Society, USA, 2010.

11. Rice, C. A. Perram, G. P. "A tunable diode laser absorption system for long path atmospheric transmission and high energy laser applications". Proceedings of SPIE, volume 7924, 79240K. 2011.
12. Rice, C. A. and Perram, G. P. "Investigation of atmospheric O₂ X³Σ_g⁻ to b¹Σ_g⁺ using open-path tunable diode laser absorption spectroscopy". Accepted for Appl. Phys. B, 2012.
13. Rice, C. A. and Perram, G. P. "A tunable diode laser absorption system for long path atmospheric transmission and high energy laser applications". Volume 7924, 79240K. SPIE, February 10, 2011 2011.
14. Rice, C.A. *Investigation Of Diode Pumped Alkali Laser Atmospheric Transmission Using Tunable Diode Laser Absorption Spectroscopy*. Air Force Institute of Technology Dissertation (AU), Wright Patterson AFB OH, 2012.
15. Rice, C.A., Lott G.E. and Perram G.P.. "Open-path atmospheric transmission for the diode pumped cesium laser," Appl. Opt. 51, 8102–8110 (2012)
16. Rothman, L. S., IE Gordon, A. Barbe, D. C. Benner, PF Bernath, M. Birk, V. Boudon, LR Brown, A. Campargue, and J. P. Champion. "The HITRAN 2008 molecular spectroscopic database". Journal of Quantitative Spectroscopy and Radiative Transfer, 110(9-10):533-572, 2009.

Vita

Matthew R. Guy graduated from Fuquay-Varina Senior High School in Fuquay-Varina, North Carolina. He completed his undergraduate studies at the United States Air Force Academy, earning an Air Force commission and Bachelor of Science degree in Physics in May of 2011. While there, he took part research centered around diode pumped alkali laser demonstration. Following graduation from the Academy, he was accepted to the Graduate School of Engineering and Management at the Air Force Institute of Technology for a Masters degree in applied physics. Upon graduation from AFIT, he will continue to an assignment to the laser research division of AFRL.

REPORT DOCUMENTATION PAGE			Form Approved OMB No. 074-0188		
The public reporting burden for this collection of information is estimated to average 1 hour per response, including the time for reviewing instructions, searching existing data sources, gathering and maintaining the data needed, and completing and reviewing the collection of information. Send comments regarding this burden estimate or any other aspect of the collection of information, including suggestions for reducing this burden to Department of Defense, Washington Headquarters Services, Directorate for Information Operations and Reports (0704-0188), 1215 Jefferson Davis Highway, Suite 1204, Arlington, VA 22202-4302. Respondents should be aware that notwithstanding any other provision of law, no person shall be subject to any penalty for failing to comply with a collection of information if it does not display a currently valid OMB control number. PLEASE DO NOT RETURN YOUR FORM TO THE ABOVE ADDRESS.					
1. REPORT DATE (DD-MM-YYYY) 21 Mar 2013		2. REPORT TYPE Master's Thesis		3. DATES COVERED (From - To) August 2012 - 21 March 2013	
4. TITLE AND SUBTITLE Investigation of the Atmospheric Propagation of Alkali Lasers in a Maritime Environment Using Tunable Diode Laser Atmospheric Spectroscopy			5a. CONTRACT NUMBER		
			5b. GRANT NUMBER		
			5c. PROGRAM ELEMENT NUMBER		
6. AUTHOR(S) Guy, Matthew R., 2 Lt, USAF			5d. PROJECT NUMBER		
			5e. TASK NUMBER		
			5f. WORK UNIT NUMBER		
7. PERFORMING ORGANIZATION NAMES(S) AND ADDRESS(S) Air Force Institute of Technology Graduate School of Engineering and Management (AFIT/EN) 2950 Hobson Way, Building 640 WPAFB OH 45433			8. PERFORMING ORGANIZATION REPORT NUMBER AFIT-ENP-13-M-12		
9. SPONSORING/MONITORING AGENCY NAME(S) AND ADDRESS(ES) High Energy Laser Joint Technology Office Dr. Harro Ackermann, Senior Technical Advisor 801 University Blvd. SE, Suite 209 Albuquerque, NM 87106 harro.ackermann@jto.hpc.mil			10. SPONSOR/MONITOR'S ACRONYM(S) HELJTO		
			11. SPONSOR/MONITOR'S REPORT NUMBER(S)		
12. DISTRIBUTION/AVAILABILITY STATEMENT DISTRIBUTION STATEMENT A. APPROVED FOR PUBLIC RELEASE; DISTRIBUTION IS UNLIMITED.					
13. SUPPLEMENTARY NOTES					
14. ABSTRACT A field deployable Tunable Diode Laser Atmospheric Spectroscopy (TDLAS) device has been used to investigate the atmospheric absorption of Diode Pumped Alkali Laser (DPAL) wavelengths at a distance of 2,000 meters in a maritime environment. The spectral regions surrounding the cesium (Cs) and rubidium (Rb) DPAL emission lines were examined in order to determine the effects of absorption by the (000)→(003) and (000)→(102) water vapor vibrational bands over a distance of 2 km. This data was compared with data previously collected at shorter path lengths and the scaling of absorbance with various factors was analyzed. Spectral data for the Cs spectral region were analyzed to determine temperature and concentration estimates with statistical errors of between 0.1 and 1.14° C and 11 and 1x10 ¹⁴ . Temperature and pressure estimates were within 6% and 25%, respectively, of those reported by the weather station at the test site. The rotational dependence of broadening rates was investigated. By analyzing the widths of two widely spaced rotational lines, it was found that the observed linewidths were approximately 25% higher than those reported in existing spectral databases with a scaling ratio of the observed rates approximately 5% below the ratio of the reported values.					
15. SUBJECT TERMS Diode Pumped Alkali Laser, Tunable Diode Laser Absorption Spectroscopy, Long Path, Maritime Environment					
16. SECURITY CLASSIFICATION OF:			17. LIMITATION OF ABSTRACT	18. NUMBER OF PAGES	19a. NAME OF RESPONSIBLE PERSON
a. REPORT	b. ABSTRACT	c. THIS PAGE			Dr. Glen Perram
U	U	U	UU	84	19b. TELEPHONE NUMBER (Include area code) (937) 255-6565, x 4504 (Glen.Perram@afit.edu)

Standard Form 298 (Rev. 8-98)
Prescribed by ANSI Std. Z39-18